AD-A090 593   NAVAL RESEARCH LAB WASHINGTON DC   F/G 20/7
              INTENSE PULSED ION BEAMS: THEIR GENERATION AND APPLICATIONS.(U)
              OCT 80   J GOLDEN, C A KAPETANAKOS, J A PASOUR
UNCLASSIFIED NRL-MR-4296   NI

END
DATE
FILMED
11-80
DTIC

(12) **LEVEL II**

NRL Memorandum Report 4296

Intense Pulsed Ion Beams;
Their Generation and Applications

J. GOLDEN, C. A. KAPETANAKOS,
J. A. PASOUR AND R. A. MAHAFFEY

Experimental Plasma Physics Branch
Plasma Physics Division

October 3, 1980

DTIC
S ELECTE D
OCT 17 1980
B

NAVAL RESEARCH LABORATORY
Washington, D.C.

80 10 16 055

REPORT DOCUMENTATION PAGE		READ INSTRUCTIONS BEFORE COMPLETING FORM
1. REPORT NUMBER NRL Memorandum Report 4296	2. GOVT ACCESSION NO. AD-A092 593	3. RECIPIENT'S CATALOG NUMBER
4. TITLE (and Subtitle) INTENSE PULSED ION BEAMS: THEIR GENERATION AND APPLICATIONS		5. TYPE OF REPORT & PERIOD COVERED Interim report on a continuing NRL problem
		6. PERFORMING ORG. REPORT NUMBER
7. AUTHOR(s) J. Golden, C.A. Kapetanakos, J.A. Pasour, and R.A. Mahaffey*		8. CONTRACT OR GRANT NUMBER(s)
9. PERFORMING ORGANIZATION NAME AND ADDRESS Naval Research Laboratory Washington, D.C. 20375		10. PROGRAM ELEMENT, PROJECT, TASK AREA & WORK UNIT NUMBERS 61153N; RR0110941; 67-0869-0-0
11. CONTROLLING OFFICE NAME AND ADDRESS Office of Naval Research Arlington, Virginia		12. REPORT DATE October 3, 1980
		13. NUMBER OF PAGES 65
14. MONITORING AGENCY NAME & ADDRESS(if different from Controlling Office)		15. SECURITY CLASS. (of this report) UNCLASSIFIED
		15a. DECLASSIFICATION DOWNGRADING SCHEDULE

16. DISTRIBUTION STATEMENT (of this Report)

DISTRIBUTION STATEMENT A
Approved for public release;
Distribution Unlimited

17. DISTRIBUTION STATEMENT (of the abstract entered in Block 20, if different from Report)

18. SUPPLEMENTARY NOTES

*Sachs/Freeman Associates, Bladensburg, Maryland 20701

19. KEY WORDS (Continue on reverse side if necessary and identify by block number)
Intense pulsed ion beams
Ion beam applications
Controlled thermonuclear fusion
Applications of pulsed power

20. ABSTRACT (Continue on reverse side if necessary and identify by block number)

The fundamentals of intense pulsed ion beam generation are reviewed. The basic processes operating in reflexing electron sources, pinched electron diodes, and magnetically insulated diodes are described. Some selected applications are surveyed; included are gas laser excitation, inertial confinement fusion, field reversed ion rings, and ion acceleration by magnetic compression.

DD $_{1 JAN 73}^{FORM}$ 1473 EDITION OF 1 NOV 65 IS OBSOLETE
S/N 0102-LF-014-6601

CONTENTS

DTIC
S ELECTE D
OCT 17 1980
B

iii

INTENSE PULSED ION BEAMS: THEIR GENERATION AND APPLICATIONS

INTRODUCTION

Out of the pulsed power technology of relativistic electron beams
have sprung a few very successful techniques for producing ultra-high
power beams of low atomic mass ions. These beams, which typically
last for less than a tenth of a microsecond, contain enough energy
to melt holes in millimeter thick aluminum plates and have sufficient
current to produce hundreds of kilogauss magnetic fields. With the
state-of-the-art power levels now approaching a Terawatt $(10^{12}W)$ and
with peak currents exceeding 0.5 Mega-Amperes, it appears that only a
modest extension of the present technology is needed to test the
feasibility of several exciting applications of these beams.

The development of ion sources has been partially stimulated by
their potential applications to controlled thermonuclear fusion programs.
Currently, there are several fusion schemes that are based on the
availability of ultra-high power ion beams. These alternate concepts
may prove to be simpler and more economical for commercial power generation
than mainline fusion approches, such as magnetic confinement fusion (MCF)
with Tokamak devices and laser-driven inertial confinement fusion (ICF).
Prominent among the alternate concepts are MCF with mirror machines
having a magnetic-field-reversed configuration produced by a rotating
ion ring, and light-ion-driven ICF. As a result of rapid advances in
the ion beam technology, preliminary tests of these alternate concepts
are already underway. If successful, these tests may lead, sometime
during the next decade, to conclusive proof-of-principle demonstrations
of these schemes, i.e., the net production of energy via fusion reactions.

In addition to their potential applications in the fusion program, intense ion beams have several other applications. Among these potential uses are: (i) the excitation of powerful gas lasers for communications, photochemical processes and research, (ii) the development of intense neutron sources for testing; and (iii) the breeding of fissile materials.

Pulsed-power technology developed rapidly in the 1960's largely to satisfy the need for intense flash-X-ray generators. By the early 1970's the technology had reached the point where high power ($\sim$24-100 GW), short-pulse (25-100 ns) generators were available at several laboratories and universities. Researchers began coupling these generators to field emission vacuum diodes to produce high current ($\sim$100 kA), high voltage ($\sim$1 MV) intense, relativistic electron beams (IREB). About 8 years ago, scientists began to realize that these generators could also be used to produce intense pulsed ion beams. Since that time, the development of ion sources has been extremely rapid. Now proton beams with currents in excess of 500 kA and current densities of 100 kA/cm^2 have been produced at voltages of 1-2 MV with pulse durations of 20-100 nsec.

Both the new sources for intense, pulsed beams and conventional ion accelerators utilize an electric field to accelerate the ions. However conventional accelerators produce continuous or long pulse beams as opposed to the submicrosecond pulses of the intense beams. As a result, conventional systems employ high voltage power supplies such as Van de Graaf, Cockcroft-Walton, and multistage tandem generators. Typical accelerating voltages are 1-10 MV, and beam currents $\lesssim$1 mA and power $\lesssim$1 kW are produced. Intense beam sources, on the other hand, are commonly powered by pulse-forming transmission lines charged by Marx generators. The short

ion pulses commonly have a 25-100 ns duration, energies of 0.1-2 MV and currents of 1 kA - 0.7 MA. Even with modest size pulse generators, ion beam power levels well above 1 GW are routinely produced.

In contrast, comparable power conventional particle accelerators (rf linacs, synchrotrons, and storage rings) operate in a higher energy regime (100 MeV - 100 GeV) than intense pulsed ion beam sources. State-of-the-art conventional accelerators have produced proton currents of 20-50 A at GeV (storage rings) and ~1 A at ~100 MeV (rf linacs). Recently, induction linacs have been proposed to generate heavy ion beams with 10kA current, 10-20 GeV energy and 10ns duration for inertial confinement fusion. However, existing induction linacs have only been used to accelerate electrons.

The development of intense, pulsed-ion-beam sources has proceeded along two different paths. The first approach is based on collective acceleration. In this approach, use is made of the negative space charge associated with an unneutralized IREB to accelerate ions. If the electron density of the beam is large enough, a sizable electrostatic potential well is formed. Positive ions with kinetic energy less than the well depth are trapped in the well, and if the well is accelerated, so are the trapped ions. The ions in such a device can attain much higher energies than the electron energy attained in the diode. Protons have been accelerated to energies 10-20 times higher than the electrons and accelerating electric fields of 1-10 MV/cm have been realized. However, the ion current in collective accelerators is generally much smaller than that of ion diodes because of the difficulties in loading the ions into the well and keeping them trapped during the acceleration of the well. The goal in current research is to extend the length over which the large

3

accelerating field acts from the few cm in present devices to a few meters. Several schemes are being actively pursued. These include (i) electron ring accelerators (University of Maryland, Max Planck Institute in Garching, W. Germany, and the Joint Institute for Nuclear Research, Dubna, USSR); (ii) wave accelerators using cyclotron or plasma waves on an IREB (Austin Research Associates, Naval Research Laboratory, Cornell University, and Los Alamos Scientific Laboratory); (iii) controlled potential wells associated with the front of a propagating IREB (Sandia Laboratories, University of California at Irvine, Lebedev Physical Institute, Naval Research Laboratory and North Carolina State University; and (iv) vacuum (Luce) diodes (Lawrence Livermore Laboratory, Air Force Weapons Laboratory, and University of Maryland). For additional information on collective ion acceleration, the reader is referred to the book by C.L. Olson and U. Schumacher. This article deals with the second, more successful approach to generating intense, pulsed ion beams that is based on the acceleration of ions within vacuum diode-like sources.

The ions originate in a plasma which is produced on the surface of the anode and are accelerated by the applied potential toward a real or a virtual cathode (i.e., a virtual surface at cathode potential). The ions form a beam and their kinetic energy is equal to ZeV, where Ze is the ion electrical charge and V is the applied potential. Normally, in such devices, most of the current is carried by the electrons because they are considerably lighter than the ions. Therefore, efficient generation of ion beams requires suppression of electron current. The details of the various methods for producing the anode plasma, extracting the ions, and suppressing the electron current (so that most of the energy is carried by the ions) are described below. Although many of the recently developed ion sources have more than two electrodes, e.g., triodes,

tetrodes, etc., the devices are generically referred to as ion diodes.

EFFICIENT ION SOURCES

In a typical field-emission IREB vacuum diode (Fig. 1) the cathode
K is connected to the negative output terminal of a pulse generator
(Marx and pulse forming transmission line). The anode A is usually spaced
approximately a centimeter away from the cathode. When the generator is
pulsed, a strong electric field (10^5 - 10^6 V/cm) develops between A and K.
This results in the field emission of electrons from microprojections
(called whiskers) on the cathode surface which have very large electric
field enhancements. For several nanoseconds these whiskers carry current,
are heated ohmically (I^2R), and eventually explode. Many such explosions
result in covering the cathode surface with a plasma. Electron emission
then occurs over the entire cathode surface. The electrons accelerate
along electric field lines toward the anode, pass through it and form a
drifting electron beam. The presence of electron space charge between
A and K modifies the applied potential and the total electric field can
be reduced to zero at the cathode. In this case the space charge limits
the electron flow across the gap. This is called Child-Langmuir flow after
the 1-D model which predicts that the current I is proportional to $V^{3/2}/d^2$,
where V is the applied potential and d is the A-K gap. In a similar
fashion, ions extracted from the plasma on the anode surface flow into
the gap. The ion space charge also modifies the electric field, and
so both the electron and ion currents are space charge limited. This
is called bipolar space charge limited flow. A one dimensional theoretical
model predicts that the current of non-relativistic electrons and ions
is given by

$$I_e = 0.093 \ (\frac{e}{m_e})^{\frac{1}{2}} \quad V^{3/2}/d^2 \qquad (e.s.u.) \qquad (1)$$

5

$$= 4.32 \times 10^{-6} \, V^{3/2} / d^2 \quad amps/cm^2 \quad (V \text{ in volts, } d \text{ in cm})$$

and

$$I_i / I_e = \{m_e / M_i\}^{\frac{1}{2}}, \tag{2}$$

where m_e and M_i are the electron and ion masses respectively.

Since the electric field is approximately zero at the electrodes, Gauss' law requires that the net electrical charge within the diode be equal to zero, i.e., $Q_e = Q_i$. Because the average current of each species is the charge divided by the residence time $\tau_{e(i)}$ within the device, the ratio of ion current I_i to electron current I_e is (Lee and Goldstein)

$$\frac{I_i}{I_e} \approx \frac{Q_i \tau_e}{\tau_i \, Q_e} \approx \frac{\tau_e}{\tau_i} \tag{3}$$

In Eq. (3) $\tau_{e(i)}$ is approximately equal to the characteristic path length $\ell_{e(i)}$ divided by the average velocity $v_{e(i)}$. For a planar diode, $\ell_e = \ell_i = d$ and $v_i / v_e = \{m_e / M_i\}^{\frac{1}{2}}$. Substitution into Eq. (3) yields Eq. (2). For protons, Eq. (2) predicts that the ratio of proton to electron current (I_i / I_e) is only 2.3%. Clearly something must be done to increase the I_i / I_e ratio if the ion production is to be efficient. According to Eq. (3) this can be accomplished by increasing the electron residence time inside the device. So far, this has been achieved by three different methods: reflexing, pinching, and magnetic insulation. In each of these three techniques, the electrons are made to travel a longer distance. Because the electrons are relativistic for most of their path length, their average velocity is a large fraction of the speed of light. Thus each of the techniques results in an increase in τ_e. However, in the case of magnetic insulation, the electron conduction current can be almost totally suppressed.

Electron reflexing devices

The first successful intense ion beam source using electron reflexing was the reflex triode shown in Fig. 2. This device usually consists of a cathode, an anode made of a thin plastic sheet which is semi-transparent to relativistic electrons, and a virtual cathode. When a positive potential pulse is applied to the anode, electrons are emitted from the cathode and are accelerated toward and pass through the anode. The space charge of the electrons that have passed through the anode modifies the applied electric field so that along a virtual surface the potential is reduced to zero. The locus of points where this occurs is called the virtual cathode. The electrons stop when they reach the virtual cathode and are accelerated back toward the anode. Since the electrons lose energy and scatter when they pass through the plastic anode, they cannot return to the cathode. Instead, they oscillate in the potential valley bounded by the cathode and the virtual cathode. With each pass through the anode, the reflection point gets closer to the anode and eventually, the electrons are absorbed in the anode.

Several nanoseconds after the electron reflexing begins, plasmas form on the surface of the anode. These plasmas are thought to result primarily from flashover discharges on the anode surfaces. Ions extracted from these plasmas are accelerated toward both the cathode and the virtual cathode. The ions which pass through the virtual cathode form a drifting ion beam. The positive potential of the propagating ion beam drags electrons from the virtual cathode. Thus, the ion beam with its comoving electrons is nearly charge and current neutral.

The reflex triode was first demonstrated in 1974 by Humphries and co-workers at Cornell University using an anode consisting of an array of

polymer or polymer-coated filaments. Improvements in anode design soon followed in experiments by Kapetanakos and Golden at NRL and by Prono and co-workers at Physics International Co. Then, in 1976, the modest power levels of these early proton beams were increased to the 0.25 TW power level (0.25 MA peak, 1.0 MV) by Kapetanakos and Golden at NRL using a coaxially configured, low inductance reflex triode. Low inductance is required if the source is to be used as a load for an ultra-high power, low impedance pulse generator.

For most of these experiments, the ratio of the extracted proton current I_p to the total current I_{total}, i.e., the proton generation efficiency ϵ, was less than 30%. This limited efficiency was primarily due to the fact that only those ions flowing toward the virtual cathode were extracted and used while the ions flowing toward the cathode were lost. If N is the number of times a typical electron passes through the anode and m_p is the proton mass, Eq. (3) gives that

$$\epsilon = \frac{I_p}{I_{total}} \approx \frac{1}{2} \left[1 + \frac{m_p/m_e^{\frac{1}{2}}}{2N + 1} \right]^{-1} . \tag{4}$$

In the limit of large N, ϵ approaches one-half. It is for large applied potential or very thin anodes that N is large. However, other factors can limit N. Fringing applied and self electric fields, and self-magnetic fields produced by the current flowing between A and K can make the electron trajectories multidimensional. The electrons then approach the anode obliquely and scatter more quickly than at normal incidence.

Another consideration is the matching of a reflex triode to the pulse generator. If N is large then a great accumulation of electron space charge piles up about the anode. This causes most of the potential drop

8

in the A-K gap to be in a region close to the anode (see Fig. 3a). The
large ion current emitted from the anode neutralizes the electron charge
so that even more electron current can be emitted. The result is a boot-
strapping effect which produces a dramatic increase in the current. However,
as the impedance drops, the load cannot remain matched to the pulse generator.
As the mismatch worsens, the load voltage drops. This eventually limits
N and I_p. This mode of operation was first reported by Prono and co-workers
at LLL and has been observed by researchers in other laboratories. It is
typical of the one-dimensional electron flow which can occur in small A-K
gaps and with large applied axial magnetic fields.

To improve upon the low efficiency of the reflex triode, a device
called the reflex tetrode (see Fig. 3b) was invented by the authors. In
the tetrode, two anodes are used. This first anode A_1 is situated between
anode A_2 and the cathode K. The material for A_1 is chosen so that plasma
formation on the surface facing the cathode is inhibited. For example,
a 6μm thick Mylar film with a few hundred Angstroms thick aluminum layer
is a poor source of plasma. Thus, there is a limited number of ions which
can flow in the A_1-K gap. The second anode A_2 is made of a thin polymer
sheet (e.g., 12.5μm thick polyethylene),which is a good plasma source.
Ions flow toward the virtual cathode and the first anode A_1. However,
the ions traveling away from the virtual cathode, arrive at A_1 with zero
axial speed and cannot pass through A_1 into the A_1-K gap. As a result,
the reflex tetrode has an approximately unidirectional flow and avoids
many of the impedance matching difficulting of the reflex triode.
Furthermore, the reflex tetrode has nearly twice the efficiency of the
reflex triode. At both NRL and Tomsk, efficiencies as high as 55% have
been achieved.

9

The impedance of the reflex tetrode is sensitive to the applied magnetic field. In addition, the quality of the ion beam is influenced by the non-uniform electric field that exists in the anode-virtual cathode gap. The non-uniformity in the field is due to the fact that the virtual cathode is not co-planar with the anode. In order to avoid these difficulties, another reflexing device, the inverse reflex tetrode (IRT) was developed (see Fig. 3c). This ion source consists of a grounded cathode screen and positively biased anode metal cylinder AC that is terminated at one end by a plate G. An anode foil A, usually a thin polyethylene sheet, is attached to the other end of the AC. An externally applied magnetic field may be used to radially confine the electron flow in the device.

When a positive pulse is applied to the anode, electrons are emitted from the stainless steel mesh cathode K, pass through the anode foil and form a virtual cathode VC between A and G. Some of the electrons are transmitted from VC to G and the rest reflex through the anode foil until they are absorbed by it or are lost to the walls of the AC. Protons are extracted out of the plasmas which form from the anode foil, probably as a result of surface flashover. These protons travel toward VC and K. When inductive effects are neglected, the potential at G is the same as that of the anode and the ion current striking G is zero. Most of the ions emitted toward K, however, pass through the coarse screen and enter the drift region. In addition, the IRT exhibits the attractive feature of

10

operating with a nearly constant impedance during an appreciable portion
of the voltage pulse. Although the ion generation efficiency of an IRT is
lower than that of a reflex tetrode, the number and average current of
protons is about 1.5 times larger, because the IRT can be better matched
to the generator. Pulses of 1-1.5 MeV protons having a peak current of
~0.5 MA, and containing $6-7 \times 10^{16}$ protons have been produced, recently,
by an IRT powered by the Gamble II Generator at NRL. The power level of
such a proton beam exceeds 0.5 TW.

Pinched electron beam diode ion sources

Another method for enhancing the ratio of ion to electron current is
to increase the electron residence time by pinching the electron flow.
Here pinching means that the electrons emitted at large radii on the
cathode move radially inward while crossing the anode-cathode gap so that
the electron flow at the anode is highly concentrated near the axis of
the device. Furthermore, pinching can be combined with reflexing to
achieve ion beams with even higher efficiency and intensity.

According to the one-dimensional, bipolar space-charge-limited flow
(Child-Langmuir) model, the diode impedance varies as d^2 where d is the
anode-cathode (A-K) spacing (see Fig. 4). However as the impedance is reduced
and the current I is increased, the azimuthal self-magnetic field B_θ becomes
larger. This self-field acts on the electron motion so that the electron
trajectories become curved rapidly inward toward the axis of the device.
At a critical value of the current, the electron velocity turns through
90° and no longer has any axial velocity component. This critical current
I_c is given by

$$I_c \approx 8500 \frac{R}{d} \sqrt{\gamma^2 - 1} \quad \text{(Amperes)}, \tag{5}$$

11

where R is the cathode radius and γ is the relativistic energy parameter

equal to the ratio of the relativistic electron mass over its rest mass.

The ratio, R/d is called the aspect ratio.

This departure from the Child-Langmuir model was observed over a decade

ago and was labelled parapotential flow, i.e., flow along potential surfaces

rather than along electric field lines. Then, in 1972-3 experiments with

high aspect ratio diodes (at NRL, Physics International Co., and Sandia

Laboratories) were conducted that demonstrated the dramatic collapse of

the electron flow. The phenomenon became known as the super-pinch and current

and power densities exceeding 10^5 A/cm^2 and 10^{10} W/cm^2 at the anode were

achieved. Often, a deep crater was blasted in the center of a "witness" target.

The role of ions in the formation of the super-pinch was not initially

appreciated. However it has been shown in a model of high aspect ratio

diodes (Goldstein, Davidson, Siambis, and Lee) that without ions in the

A-K gap, only weak pinching occurs. The electrons emitted at the cathode

radius R arrive at the anode at a radius of approximately R/γ. Experiments

at NRL and Sandia have shown that the rate of collapse of the electron flow

towards the axis depends on the rate of anode plasma production. It

is from this plasma that ions are extracted and accelerated towards the

cathode. Computer simulations at NRL and Sandia Labs have shown that the

ions act to neutralize the negative space charge of electrons in particular

near the anode and the vicinity of the axis. This permits a larger current

and therefore a stronger magnetic field in the device. More importantly,

it allows the electrons to move in a nearly radial direction in the vicinity

of the anode. Consequently, the ratio of ion to electron current I_i/I_e

for bipolar planar flow is enhanced by the ratio R/d when strong pinching

occurs, and Eqs. (3) predicts:

$$\frac{I_i}{I_e} \geq \frac{R}{d} \frac{\beta}{2} \quad , \tag{6}$$

where β is the ratio of the ion velocity at the cathode to the speed of light. Since the electrons are relativistic, β is approximately the ratio of the ion and electron velocities. For a large aspect ratio and high voltage V, this ratio is near unity. For example, with $R/d \sim 30$ and $\beta \sim 1/20$ (corresponding to $V \sim 1.2$ MV) Eq. (6) predicts $I_i/I_e \sim 0.75$.

By using an annular cathode or a thin polymer foil cathode, the ions flowing across the A-K gap can be extracted through the cathode as a beam. Pinched electron diodes have been successfully used to generate ion beams by researchers at NRL (Stephanakis, et al.), Sandia (Johnson et al.). Cornell (Hammer et al.), and Physics International Co. (Genaurio, et al.).

Experiments have shown that by using a thin anode foil, some reflexing will take place along with the pinching. This combined action further increases the electron residence time. In recent experiments performed by a collaboration of researchers at Physics International Co. and NRL, beams of protons or deuterons have been produced having a current of one MA and an energy of two MeV corresponding to an ion beam power of two Terawatts. Furthermore, because of the intense flow of electrons near the axis, these diodes appear to be well suited to the production of high current density, solid beams. Using a hemispherically shaped anode and cathode, Stephanakis, and co-workers at NRL have produced ballistically focused proton beams with a peak current density exceeding 100 kA/cm^2.

Magnetically Insulated Diode Ion Source

The third type of ion source, the magnetically insulated diode MID, employs a magnetic field parallel to the electrode faces to prevent electrons from crossing the anode-cathode gap. If the electron current is almost completely

suppressed, then it is possible to obtain a very high ion production effi-
ciency. The minimum magnetic field required for turning an electron around
before it reaches the anode is given by

$$B^* = \left(\frac{m_o c}{e}\right) \{\gamma^2-1\}^{\frac{1}{2}}/d \qquad (7)$$

where d is the electrode spacing, e and m_o are the charge and mass of an elec-
tron, and c is the speed of light. As an example, if V = 1 MV and d = 1 cm,
then $B^* = 5$ kG. Since the ions to be accelerated across the gap are much more
massive than the electrons, their gyro-radius in the applied field is much
larger and they cross the diode while undergoing only slight deflection.

Ion generation by magnetically insulated diodes was first proposed by
Winterberg and later by Rostoker and then by Sudan and Lovelace. The devices
were developed at Cornell University by Humphries and coworkers and have been
operated at high power levels at Sandia Laboratories where Johnson and co-
workers have produced ion beams of 100 kA/cm^2 at 2 MV with 80% efficiency.

A planar magnetically insulated diode is illustrated in Fig. 5. Ions are
extraced from the diode through the cathode, which may be a wire mesh or a
metal plate with openings to let the ions pass through. Great care must be
taken in constructing a MID to keep the magnetic field lines parallel to the
electrode surfaces. If a field line intersects both the anode and the
electron sheath, then electrons can stream along that field line, thereby
shorting the diode.

Besides their inherently high efficiency, another attractive feature
of magnetically insulated diodes is that the anode is reusable, at least
when it is coupled to a moderately powered generator. The anode typically
contains dielectric inserts which form plasma by surface breakdown when
the diode voltage is applied. During the pulse, relatively little energy

14

is deposited in the dielectric, so it suffers relatively minor damage. There can, however, be substantial damage after the main pulse when the cathode plasma diffuses across the magnetic field and strikes the anode.

For very large applied magnetic fields ($B_o \cdot \cdot B^\ast$), the electrons are confined very close to the cathode and the extracted ion current is limited to the Child-Langmuir value. However, if B is only slightly larger than $B^\ast$, the electron charge is enhanced because the electrons move closer to the anode. Consequently, the ion current is enhanced. This behavior has been predicted theoretically (Bergeron; Antonsen and Ott) and observed experimentally. Ion current densities 5-10 times above Child-Langmuir have been obtained. MID's are attractive for long pulse operation because the applied magnetic field also acts to impede plasma motion across the gap. In the microsecond long pulse experiments of Luckhardt and Fleischman at Cornell, these enhanced ion current densities have resulted in the production of 4.5×10^{13} protons/cm^2. Table 1 gives the State-of-the-Art of pulsed ion sources.

For several applications (e.g., inertial confinement fusion), it is necessary to focus the ion beam to a diameter of ~ 1 cm. Spherical magnetically insulated diodes have been used to provide such focusing. In a spherical diode, ions emitted from the anode converge at the center of the diode, resulting in a large gain in current density. In experiments at Cornell and Sandia, gains in ion current density of ~ 20 have been achieved. However, for an inertial confinement fusion reactor, ions must not only be focused to a small diameter,

15

but they must also be transported over a distance of several meters to the fusion pellet. Otherwise, the blast from the fusion reaction will destroy the diode.

DIAGNOSTICS FOR INTENSE ION BEAMS

It became evident even during the initial development of intense ion beam sources, that many diagnostic techniques which had been successfully used to probe electron beams are not applicable to intense ion beams. The main reason is that intense ion beams are at least partially space-charge and current neutralized by co-moving electrons. These traits preclude several electrical measurements, such as charge collection and current or self-magnetic field measurements.

Many of the techniques presently available to measure the properties of these beams (see Table 2) have been adapted mainly from nuclear physics.

One of these methods, which has been applied successfully to intense ion beams is nuclear activation analysis. For more details see the review paper by F.C. Young, J. Golden and C.A Kapetanakos, Rev. Sci. Instrum. 46, 432 (432). Presently, this is the most unambiguous means for the determination of the number, identity, and spatial distribution of light ions.

Nuclear activation analysis is based on the measurement of the number of radio-active nuclei induced in a target by the ion beam. In the case of protons and deuterons, reactions occur in the elements ^{10}B, ^{12}C, and ^{14}N which lead to radioactive nuclei that have half-lives of a few minutes and that decay by emitting a positrons (see Table 3).

By counting the coincident γ rays resulting from the subsequent annihilation of the positrons, and correcting for the decay during the

16

time between activation and counting, the number of radio-active nuclei induced in the target can be determined. For many reactions, the thick target yield, i.e., the number of reactions produced per incident ion striking a thick target is known. The number of incident ions is equal to the number of radioactive nuclei produced divided by the thick target yield.

A similar approach is to monitor the neutrons produced by (p,n) or (d,n) reactions induced by the ions in suitable targets. A list of some of the more useful neutron-producing reactions is also included in Table 3. This technique has the important advantage that some of the neutron-producing reactions have moderate yields at energies which are below the resonances or thresholds of the residual-radio-activity-producing reactions. The main disadvantages with this technique is the sensitive dependence of the (p,n) and (d,n) reaction cross section on the energy of ions.

An alternative technique is to monitor the prompt radiation, i.e., γ rays or neutrons, produced by the ion induced nuclear reactions. The prompt γ-rays can be detected by fast response scintillators attached to fast recovery, high-saturation-current photomultipliers. High yield reactions that have proved to be useful are the $^{19}F(p,\gamma)^{16}O$ and the $^{7}Li(p,\gamma)^{8}B_{e}(\epsilon)$ reactions. It is important that an appropriate reaction is selected with yield that does not vary much over the energy range of the ion beam. In this case, the prompt γ-ray signal is proportional to the ion current. When the absolute calibration of the detector is not available, the prompt γ-ray signal can be normalized to the number of ions in the pulse measured via another technique, e.g., activation analysis of residual radioactivity in a target. Prompt γ-ray measurements

also require that care be taken to avoid interference by x-rays which are generally produced by high energy electrons at the ion source. Spatial or temporal separation of the prompt γ-ray and x-ray pulses is usually required.

A useful tool for measuring the time of flight and the shape of the ion pulse is a detector consisting of a thin scintillator coupled optically to a fast photodiode by a long acrylic light-pipe encased in a stainless steel tube. A vapor deposited layer of aluminum 0.2 - 1.5μm thick shields the detector from extraneous light. For current densities greater than a few hundred A/cm^2 screens must be used to attenuate the beam and thus prevent destruction of the aluminum and scintillator.

Recently, another method has been demonstrated which gives information about the spatial distribution and number of protons in the pulse. This diagnostic suggested by Bleach and Nagel at NRL, and adapted to intense ion beams by E. Burns and co-workers at Sandia and F.C. Young at NRL, consists of monitoring the soft x-rays emitted when a proton beam strikes a metallic target. The line radiation of a few kilovolts energy is produced from the excitation of inner shells (K,L,M) of a suitable target as for example aluminum. This radiation can be detected with x-ray diodes (XRD) or by x-ray pinhole photography. By calibrating the XRD or the pinhole-camera film system, and from the known cross-section for excitation of the x-ray lines, the dose of ions on the target can be determined.

Presently many of the diagnostic methods available for intense ion beams suffer from serious limitations. For example, with nuclear activation analysis, a major problem is "blow-off" of the target. The beams can be so intense that the surface of the target bearing the radioactivity induced by the beam can be heated to melting or even ablated so that the radioactive nuclei are lost prior to detection. Although prompt γ-ray detection may avoid the problem of blow-off, it is usually

18

complicated by the interference of x-rays and the lack of knowledge of the ion energy distribution.

For intense fluxes of ions with energi s below the thresholds or resonances for the reactions amenable to nuclear activation analysis or prompt radiation detection, a reliable diagnostic method is not available. Nuclear activation techniques based on resonant reactions cannot be used for light ions with energies below 200 keV per AMU. Etched tracks in films or emulsions have been used with ion beams at many laboratories, but this method is strictly limited to low fluxes.

Biased ion collectors (BIC) have often been used to measure the current of low energy ion beams. These charge collectors usually consist of a cup connected in series with a low-Ohmic resistive element enclosed in a shielded container. For an electron beam, the current incident on the collector can be determined by measuring the voltage developed across the resistive element. Secondary electron currents are conveniently suppressed by the negative space charge that is developed by the primary electrons in front of the collecting surface. However, for an ion beam, the electrons co-moving with the ions neutralize the beam current. Biasing the collector negatively retards the electrons, but the bias potential also accelerates the secondary electrons produced by the ions on the surface of the collector. Because the secondary emission coefficient of ions in the energy range 0.1-1 MeV is typically greater than unity (especially for oblique incidence), the contribution of the secondary electron current to the measured current can be quite large. These difficulties can be partially avoided by using collectors with small apertures and a magnetic field parallel to the collecting surface to reduce the secondary electron flow.

19

SOME SELECTED APPLICATIONS OF INTENSE ION BEAMS

In the following sections, we review the concepts and the present status of some promising applications of intense ion beams. The recent impressive advances in the generation of ion beams suggest that in the near future ion beams will be available at power levels required for the thermonuclear fusion oriented applications of such beams. At the present power level, ion beams have been used at NRL to form transient field-reversed ion layers and to excite high power gas lasers. In addition, MeV energy ion beams have been focused to current densities in excess of 100 KA/cm^2.

(a) P-beam Excitation of Lasers

The envisioned uses of gas lasers include drivers for inertial confinement fusion, isotope separation, and undersea communications and sensing. As described in a recent article reviewing gas laser technology (J.G. Eden, et al., Spectrum, April '79), the gas lasers to be used in these applications must have high power and efficiency. These requirements also apply to the means of putting energy into the gas, i.e. the excitation source, or more simply "the pump".

Many lasers of current interest, e.g. the excimer lasers, use an intense pulsed relativistic electron beam as the pump. Typically these lasers rely on the ionization of a rare gas by the e-beam to ultimately create the upper state population of the laser. However, as pointed out by A.W. Ali at NRL (1977), the use of proton beams for laser excitation appears attractive because the ionization per unit path length by protons in rare gases is greater than that produced by electrons of the same energy. However, the advantage of protons over electrons resulting from the high energy deposition per unit volume of protons must be balanced against the lower efficiency with which proton beams can be produced

20

and delivered to the gas.

In comparison with e-beam pumping, it is expected that p-beam pumped lasers may operate at lower gas pressures at which absorption by the diluent gas is reduced. Alternately, higher ionization densities may be achievable at a given pressure, and so more compact, new, or more efficiently pumped lasers may be possible.

Experiments at NRL have been performed which demonstrated p-beam pumping of N_2 and XeF molecules. The apparatus for these experiments is shown schematically in Fig. 6. The proton source was a reflex tetrode which produced a 450 keV proton beam with current density of ~10A/cm^2 and 50 ns duration. The beam was passed through a thin Mylar foil (3μm thick) into a gas mixture of about 1 atm pressure. An optical cavity was formed by two spherical mirrors external to the gas cell, and a magnetic field was used to improve the performance of the reflex tetrode and to help transport the beam to the gas cell.

The first demonstration of a p-beam excited laser was achieved in 1978, when stimulated emission at 357.7 and 380.5 nm was observed in a Ar/N_2 gas mixture. In further experiments, p-beam pumping of the XeF laser, one of the promising rare-gas-halide lasers, was studied. In this UV laser, the dependence of output energy on the input energy and also on the transmission of the output mirror (i.e., the coupling) was measured. Many similarities with e-beam pumping have been observed. However, unlike the e-beam pumped XeF laser, helium could be successfully used as a diluent gas with p-beam pumping. At 1 atm gas pressure (97% Ar/2.6% Xe/0.4 NF_3) the efficiency was found to be ~2.7% when the output coupling was 6%.

Although these preliminary results are promising, in order to achieve higher power levels, a number of problems must be overcome. As with e-beam pumping, there is a limit on how much ionization and

energy deposition can be efficiently utilized. At very high pump powers, processes occur which can destroy the upper laser level population because of the higher deposition for protons, these processes may restrict the maximum useful p-beam current density.

Apart from the detailed kinetics, there are also technological problems that include the loss of proton energy in the foil window, the support of a thin foil against a gas pressure of several atm, matching the p-beam shape with a practical laser shape, and finally, coping with the large laser output power densities which are expected because of the compactness of p-beam pumped lasers. It appears that most of these difficulties can be minimized by utilizing protons with higher energy, i.e., in excess of 1 MeV. The increase in proton range with higher energy permits the use of thicker foils with a lower energy loss in the foil.

Increased range also permits a larger laser aperture to be used. For a given laser output power, the power density can be reduced so that damage to the laser mirrors may be avoided.

(b)   Inertial Confinement Fusion

The product of density and plasma confinement time required for a 10 keV plasma by the Lawson criterion for fusion breakeven can be achieved by confining a low density plasma for a long time (e.g., density $n_p = 10^{14}/cm^3$, confinement time $\tau_c = 1$ second), as in magnetic confinement fusion devices (i.e., tokamaks and mirror machines) or by confining a very dense plasma for a very short time. The latter is the approach followed by inertial confinement fusion (ICF). In order to obtain the required $n_p \tau_c$, a hollow pellet a few millimeters in diameter filled with a deuterium and tritium mixture must be compressed to a density $\sim 10^{24}/cm^3$ for less than

a nanosecond (see Fig. 7). This means that the gas within the pellet must be compressed by a factor of about 10^5 to a density more than 100 times solid density. Compression can be achieved by irradiating the outer layer of a pellet so that it explosively ablates. This ablator imparts inward momentum to an inner shell (sometimes called a pusher) which is driven inward and compresses the DT fuel. The inward inertia of the interior shell or shells provides confinement and hence the name ICF. The means used for delivering the momentum to the pellet is called the driver.

Presently, lasers, electrons, light ions, and heavy ions are being investigated as drivers. Lasers are the leading candidates because extremely short pulses of high power laser radiation can be easily focused onto the small pellets using systems of mirrors and lenses. Lasers, however are more expensive and inefficient than particle beams. They currently cost about $500/Joule and at least 1 MJ is required for energy breakeven. The two leading ICF candidate lasers are neodymium-glass lasers which have efficiencies less than 1% and carbon dioxide lasers which have efficiencies less than about 10%. On the other hand, heavy ion beams accelerators may have very high efficiencies but they also are expected to have high capital costs. In contrast, light ion or electron beam generators can have an efficiency of 25-50% and a moderate cost of $10-$100/Joule.

There exist major technological problems which have to be overcome if particle beams are to be viable drivers for ICF. These problems include the generation of particle beams at the power level of 10^{14} Watts, transporting such beams away from the source, focusing them onto the target and operating pulsed power generators at high repetitive rates and high average power. To compress a pellet, it is necessary to deposit the

energy close to the surface of the pellet, e.g., in the ablator. If too much energy is deposited deep inside the pellet, then the inwardly moving material must push against the pressure exerted by the heated inner region. This problem is called preheating.

Electron beam drivers are limited to energies below a few MeV in order to avoid preheating. Even with the use of the self-magnetic field of the beam to reduce the range of the electrons and stop them in a thin outer layer of the pellet (an effect observed by researchers both at I.V. Kurchatov Institute, USSR and at Sandia Laboratories), an electron beam of less than 3 MeV energy and power in excess of 100 TW is needed. As a result, the beam producing pulse generator must have an impedance which is considerably less than one-tenth of an Ohm. Such a low impedance poses some extraordinary technological difficulties for both the pulse generator and the transport of the beam from the source to the pellet.

Although substantial progress has been made in developing the technological solutions to these problems, ion beam drivers appear to be an attractive alternative. For charged particles of the same energy, more massive particles have a shorter range. Therefore, ions with higher energies can be used instead of electrons. Consequently, the pulse generator used to produce the ion beam can have a higher impedance. For example, models by Clauser at Sandia Laboratories predict that a net-energy-breakeven demonstration of ICF could be performed with a 10 MeV, 10 MA proton beam. Beams with such parameters could be obtained with a pulse generator having an impedance of about 1 Ohm.

Another reason for using an ion beam driver is that ion sources can be made in which the ions carry most of the current in the device. Pinch-reflex diodes studied by Cooperstein and co-workers at NRL produce

24

a $\sim$1 TW proton beam with $I_i/I_{total} \sim$ 0.6. It is expected that for this type of source, the ion generation efficiency will improve with an increase in the power level. Also magnetically insulated diodes can have high efficiencies. Johnson et al. at Sandia Laboratories has recently reported a MID having $\sim$ 80%.

In order to compress a pellet to thermonuclear conditions, a 100 TW beam must be delivered to the pellet with a power density of $\sim$ 30-100 TW/cm^2. A beam of 10 MeV ions must have a current density at the pellet of $\gtrsim$ 3 MA/cm^2. To obtain this, the ion beam must be focused onto the pellet. Several focusing methods have been proposed and are experimentally investigated at NRL, Cornell University, and at Sandia Labs. These include ballistic or geometric focusing using curved diode electrodes and self-focusing using the azimuthal self fields.

Because of the azimuthal self-magnetic field produced by the electron and ion currents in the diode and that produced by the propagating beam, self-focusing can occur even when the beam is generated in a planar diode. In addition, when curved electrodes are used, the electric field in the A-K gap has a radial as well as an axial component. By properly shaping the electrodes, the amount of radial force exerted on the ions can, in principle, be adjusted so that the ion trajectories converge. This focusing has been demonstrated by Cooperstein and co-workers at NRL using a pinch reflex diode having spherically curved electrodes. By injecting the beam into a short gas-filled drift region ($\sim$1 Torr), plasma was produced which facilitated the current neutralizing of the ion beam. This allowed the beam to drift force-free to a focus a few cm from the diode. By measuring the neutrons from D-D reactions induced by a deuteron beam in small CD_2 targets, they inferred peak deuteron current densities of 200 kA/cm^2.

At Sandia Labs, Johnson et al. used geometric focusing of beams produced in an annular, curved electrode MID to obtain focused ion beams with peak current densities well above $100kA/cm^2$.

It is also necessary that the ion beam be propagated a distance (~1 m) away from the generator because the intense radiation flux from the thermonuclear reaction can damage the generator. Various methods of transporting the ion beams are being investigated at NRL and at Sandia Labs.

In one approach, the beam is transported through a small-diameter plasma channel. One technique for establishing such a channel is to explode a thin (typically ~50μm diameter) wire by discharging a capcitor through it. As much as 50% of an ion beam has been propagated over 0.5m in experiments by D. Mosher and co-workers at NRL. The problem with this technique is that the background gas pressure must be kept low in order to minimize (dE/dx) losses. However, at low background pressure, the channel tends to be subject to plasma instabilities which can disrupt beam transport.

Another technique for establishing the plasma channel is to strike a z-discharge in a neutral gas. Experiments have been performed by F. Sandel at NRL using 0.2-2 Torr pressure of N_2 or He gas. So far, most of the particles have been transported as far as 1 m, but there is an energy loss. This loss amounts to about 200 keV of the initial 1.4 MeV ion energy. The energy loss mechanism is still being investigated. Other techniques have been proposed for producing the plasma channel. For example, plans are being made at Sandia Labs to use laser initiated discharges.

Although very high ion current densities have already been achieved, an additional factor of 30 in the beam power density is still needed. Part of the required increase in power may be obtained by bunching the ions within a pulse. This can be accomplished by applying a temporally increasing potential to the ion source. As the faster ions at the end

of the pulse catch up to the front of the pulse, the beam pulse will shorten but the power will increase. This bunching along with the overlapping of several beams may yield the necessary power for light ion-beam driven ICF.

(c) Field Reversed Ion Rings

Perhaps the most significant application of intense, pulsed ion beams is the formation of field reversed ion rings. Such rings can be formed by trapping a large number of energetic ions in a magnetic mirror field. When the diamagnetic self field of the symmetry axis encircling ions exceeds the applied magnetic field, the total magnetic field in the interior of the ring reverses direction. As a result the magnetic field lines close, as shown in Fig. 8.

Field reversed configuration generated by energetic charged particles provide an ideal configuration for confining plasmas for thermonuclear applications for the following reasons: (i) the plasma confinement time is considerably enhanced because the trapped plasma would have to cross the closed magnetic field lines in order to escape, (ii) the gyrating particles of the ring serve as an internal energy source for heating the confined plasma, and (iii) the beta (β) of the plasma

$$\left[\beta = \frac{\text{plasma pressure}}{\text{external magnetic field pressure}} \right]$$

can exceed unity and thus the power density of a thermonuclear reactor can be high. As a result, the size of the reactor can be appreciably reduced resulting in very significant economic benefits.

Although under actual laboratory conditions the ensemble of gyrating ions will have a shape that closely resembles that of a ring, for simplicity consider a long rigidly rotating layer. If a_1 is the inner and a_2 the outer radius of a space charge neutral layer that rotates with a constant

27

angular frequency ω around its axis of symmetry, the ratio of the total magnetic field in the interior of the layer $B_z(r)$ to the applied magnetic field B_o is given by

$$\frac{B_z(r)}{B_o} = 1 + \frac{2\omega\nu}{\Omega_o}\left[\frac{(a_2^2 - r^2)}{(a_2^2 - a_1^2)} - \frac{(a_1^2 + a_2^2)}{2b^2}\right] \tag{8}$$

where $\Omega_o = \frac{qB_o}{mc}$ is the cyclotron frequency corresponding to the applied field, q and m are the charge and mass of gyrating particles, ν is the Budker parameter and b is the radius of a perfectly conducting wall that surrounds the layer. The magnetic field for $r \leq a_1$ and $a_2 \leq r \leq b$ is constant and may be found by letting $r = a_1$ and $r = a_2$ in Eq. (8) respectively. Figure 9 shows the ratio $B_z(r)/B_o$ as a function of radial distance for different values of ω/Ω_o. Note that this combination of parameters is always negative because ω is negative when Ω_o is positive and vice versus. The Budker parameter $\nu = \frac{q^2}{mc^2} \bar{n}\pi(a_2^2 - a_1^2) = \frac{q^2}{mc^2} N_\ell$, i.e., is the product of the charged particle per unit length N_ℓ and is of fundamental importance in the theory of reversed field configurations.

The last term in Eq. (8) is due to induced currents (eddy currents) on the wall of the conducting cylinder surrounding the layer and becomes zero when the conductor is removed ($b \to \infty$).

The field reversal factor $\eta = B_z(a_1)/B_o$ may be found from Eq. (8) by letting $r = a_1$ and using the relation $\Omega(\rho) = \frac{qB_z}{mc} = -\omega$, where $\rho = \sqrt{(a_1^2 + a_2^2)/2}$. After some simple algebra, it is obtained $\eta = \frac{|\omega|}{\Omega_o}(1-\nu)$. Therefore, field reversal cases requires a Budker parameter that exceeds unity. Since the Budker parameter is inversely proportional to the mass of the gyrating charged particles, considerable more ions are required to form a field reversed configuration than electrons. However, reversed field

configurations that are generated by electrons are not of interest for thermonuclear applications because of the synchrotron radiation losses from the fast moving electrons. Therefore, only protons or heavier charged particles can be used in the formation of field reversed layers or rings that have applications in the fusion program. Since ~ 1 for field reversal, the number of protons per unit length required is $N_\ell = (q^2/mc^2)^{-1} = 0.64 \times 10^{16}$ cm^{-1}. This number is very large and generally can be obtained only with the recently developed pulsed ion sources.

Presently, there are two experimental programs, one at NRL and the other at Cornell University, that are aimed toward the generation of a reversed field configuration with proton rings. A schematic of the NRL ion ring experiment is shown in Fig. 10 and a photograph of the same experiment is shown in Fig. 11. In the most recent experiment, the applied magnetic field consists of a short uniform region, a magnetic cusp, a 75 cm long uniform field and a single magnetic mirror. The Inverse Reflex Tetrode (IRT) proton source is located in the short uniform field and is powered by the upgraded Gamble II generator. This source generates a hollow, ramp-shaped proton pulse that contains more than 6×10^{16} protons of about 50 nsec base line duration. Typically, the peak of the applied voltage on the source is 1.5 MV.

After propagating in the short uniform magnetic field, the hollow proton beam enters the magnetic cusp, where it starts to rotate as a result of $v_z B_r$ force. The self magnetic field of the layer is monitored with several magnetic probes that are located on axis and near the wall.

The first transient field reversal ever obtained with ions was achieved at NRL in the Spring of 1979. Presently, experiments are under way to trap the protons with the aid of a gate field that is located at the beginning of the 75-cm long uniform field.

29

The simplified condition for self-sustained thermonuclear reactors (Lawson criterion) is $n_p t_c \cdot 10^{14}$ cm^{-3} sec, where n_p is the plasma density and τ_c is the plasma confinement time. Since the plasma is mainly confined by the self magnetic field of the ion ring, the life time (τ) of the ring should be longer than the plasma confinement time t_c. The life time of the ring is mainly determined by the interaction of ions with the plasma electrons and is given by

$$\tau = 0.59 \times 10^{12} \; (m_p/m_i)^{\frac{1}{2}} \frac{W^{3/2}}{n_e} \quad ,$$

where n_e is the electron density in cm^{-3}, W is the ion energy in MeV, m_p is the proton mass and m_i is the mass of ions that make up the ring. For protons ($m_i = m_p$), the energy W must be about 35 MeV in order to have $n_e t_c$ greater than 10^{14} cm^{-3} sec. Since during trapping the energy of protons is between 1 to 2 MeV, a twenty-fold increase in their energy is required.

(2) Inductive Acceleration of Ions by Adiabatic Magnetic Compression

A convenient way to increase the energy of gyrating ions is by adiabatic magnetic compression of the ring.

When an axial magnetic field $B_z(t)$ increases with time, an azimuthal electric field $E_\theta(t)$ is induced which enhances the energy W of a particle of charge q at the rate

$$\frac{dW}{dt} = q V_\theta E_\theta \quad ,$$

where V_θ is the instantaneous azimuthal velocity of the gyrating particle. If the self fields are neglected, and the magnetic field changes slowly

in time (adiabatic) then the magnetic moment $\mu = \dfrac{W(t)}{B(t)}$ of a gyrating ion is conserved and thus its energy increases proportional to the applied field $B(t)$.

In the presence of self fields, the energy of ions increases slower than that predicted for a single particle because a portion of the externally supplied energy goes into thermal energy and also into self-magnetic energy of the ring.

The inductive acceleration of ions can be used either to increase the energy of the ions and thus to extend their life time in a thermonuclear reactor or it can be used in the generation of high energy, high current ion pulses. In the latter case the ring must be unwound into a straight beam after compression. A way to accomplish this is by opening the far mirror peak and passing the rotating ring through a half cusp as shown in Fig. 12. Equilibrium states for this space charge neutral, rotating-propagating hollow beam exist even in the absence of an external magnetic field, because the outward directed centrifugal and $J_\theta B_z$ forces are balanced by the $J_z B_\theta$ force. The magnetic forces $J_\theta B_z$ and $J_z B_\theta$ are due to the self fields B_θ and B_z of the beam and are generated from its axial J_z and azimuthal J_θ currents.

Table 4 shows the parameters of a ring before and after compression. It must be emphasized that the 0.91 Megagauss peak value of magnetic field is rather conservative since magnetic fields in excess of 1.3 Megagauss have already been generated by flux compression using metal liners. The predicted 100 MeV ion energy at the peak of the compression is based on the assumption that the self fields are small and thus μ is conserved during compression. When the purpose of the compression is the generation

31

of high energy beams, the self fields can be kept appreciably smaller than
the applied field by partial cancellation of the ion current by an electron
return current. Such a partial cancellation is highly desirable because
it allows efficient transfer of the externally supplied magnetic energy
into particle kinetic energy during compression.

The usefulness of ion rings in the fusion program and also in the
generation of high energy ion pulses rest very heavily on their stability.
As a result of the complexity of the problem, no comprehensive treatment
of the stability of field reversed rings is presently available. However,
results obtained so far are very encouraging.

Using the energy principle Sudan and Rosenbluth have shown that a
field reversed ion ring is stable against MHD kinking modes when its aspect
ratio r = major radius/minor radius is near unity. Lovelace has arrived
at a similar conclusion.

Tearing modes, i.e., instabilities that break up a long layer into
several rings can be avoided by surrounding the layer by a close fitting
conducting wall (Marx) or by introducing a spread in the axial velocity of
the ions (Fowler; Uhm and Davidson). The latter has been confirmed in
recent computer simulation experiments by Marsh and Drobot.

Similar conclusions have been reached about specific instability
modes. For example, Uhm and Davidson have treated the stability of a
field reversed layer for frequencies near multiples of the mean rotational
frequency of the layer. Such instabilities are of primary concern. They
have found that in the presence of a dense background plasma the system
can be easily stabilized by introducing transverse temperature in the
layer's ions.

THE NEXT FEW YEARS

The turning point for intense, pulsed ion beams may come during the next 3-4 years. If the remarkable rate of success of the last 3 years is continued then a number of significant accomplishments may be achieved. In the area of laser excitation, demonstrations of higher power and higher energy UV and new blue-green p-beam pumped lasers are already being planned.

During 1981-1982, the particle beam fusion accelerator (PBFA) will come on-line at Sandia Labs. If solutions to the ion beam transport and focusing problems are found, then in the mid-80's ion beams will be used as drivers in an attempt to demonstrate ICF breakeven. Finally, efforts to trap a field-reversed ion layer in a magnetic mirror are in progress at NRL. If these experiments are successful, then the prerequisite for field-reversed mirror machine fusion devices and inexpensive relativistic ion accelerators will be at hand. Although the success of any of these ion beam applications is by no means certain, the possible high pay-offs are the investment in ion beam research a good bet.

REFERENCES

Ion Sources

Triodes:

J. Golden, C.A. Kapetanakos, S.J. Marsh, S.J. Stephanakis, Phys.
Rev. Lett. 38, 130 (1977).

Tetrodes:

J.A. Pasour, R.A. Mahaffey, J. Golden, C.A. Kapetanakos,
Phys. Rev. Lett. 40, 2143 (1978).

Inverse Reflex Tetrodes:

J.A. Pasour, R.A. Mahaffey, J. Golden, and C.A. Kapetanakos,
Appl. Phys. Lett. 36 646 (1980).

Pinched beam diodes:

S.J. Stephanakis, D. Mosher, G. Cooperstein, J.R. Boller,
J. Golden, and S.A. Goldstein, Phys. Rev. Lett. 37, 1543 (1976).

Magnetically insulated diodes:

J. Maenchen, L. Wiley, S. Humphries, Jr., E. Peleg, R.N. Sudan,
and D.A. Hammer, Phys. Fluids 22, 555 (1979).

D.J. Johnson, G.W. Kuswa, A.V. Farnsworth, Jr., J.P. Quintez,
R.J. Leeper, E.J.T. Burns, and S. Humphries, Jr., Phys. Rev.
Lett. 42, 610 (1979).

Collective acceleration:

C.L. Olson, U. Schumacher, Collective Ion Acceleration, Springer Verlag,
Berlin (1979).

Particle beam fusion:

G. Yonas, Sci. American, 239, 50 (1979); also IEEE Transactions on
Nuc Sci NS-26, 4169 (1979).

Diagnostics:

F.C. Young, J. Golden, C.A. Kapetanakos, Rev. Sci. Instrum., 48,
432 (1977).

Theory; (mainly electron beams)

R.C. Davidson, Theory of Non-Neutral Plasmas, W.A. Benjamin, Inc.,
Reading, Mass. 1974.

Appendix I — INTENSE ION BEAM RESEARCH

Where it's happening

Naval Research Laboratory (NRL), Washington, D.C.

  (Ion Ring Group) reflexing sources, rings, lasers, accelerators, diagnostics; experiment and theory

  (Ion Beam Group) pinched electron diodes, transport, focusing, diagnostics; experiment and theory

Sandia Laboratories, Albuquerque, New Mexico

  light-ion-drivers for ICF, magnetically insulated diodes, diagnostics, ion accelerators; experiment and theory

Cornell University, Ithica, New York

  Magnetically insulated diodes, focusing, rings, lasers; experiment and theory (2 groups)

Lawrence Livermore Laboratory, Livermore, California

  Reflexing sources; experiment and theory

Physics International Company, San Leandro, California

  Reflexing sources, pinched electron diodes

University of California, Irvine, California

  Reflexing sources, magnetically insulated diodes, injection into a torus; experiment

University of Illinois, Urbana, Illinois

  Ion rings; theory

University of Maryland, College Park, MD

  Pinched electron diodes, reflex sources; theory

Nagoya University, Nagoya, Japan

  Reflexing sources; experiment and theory

Massachusetts Institute of Technology, Cambridge, MA

  Reflexing sources, ion rings; experiment and theory

University of Michigan, Ann Arbor, Michigan

    Ion rings; theory

Weizman Institute, Rohoboth, Israel

    Pinched electron diodes; experiment

Institute of Nuclear Physics, Tomsk, U.S.S.R.

    Reflexing sources, laser excitation with p-beam; experiment

Lebedev Institute, U.S.S.R.

    Reflexing sources; experiment

Harry Diamond Laboratory, White Oak, MD

    Reflexing sources; experiment

Auburn University,

    p-beam pumped lasers; experiment

Table 1 — State-of-the-Art of Pulsed Ion Sources

Source	V(MV)	I(KA) ion peak	DURATION (ns)	LABS.
reflex triode	1.2	200	50-60	NRL
	0.3	150	160	LLL
reflex tetrode	1.2	250	50-60	NRL
IRT	1.5	500	50-60	NRL
Pinched electron diode	1.3	700	50-60	NRL
	2.0	1000	---	PI
MID	2.0	400	85	Sandia Lab.

Table 2 — Diagnostics for Intense Ion Beams

Beam parameter	Diagnostics
Number of ions/pulse	(i) Nuclear activation analysis (ii) Spectroscopy of ion induced x-rays (iii) Tracks in nuclear emulsions
Spatial distribution of ions	(i) Nuclear activation analysis with segmented targets (ii) Photography of ion induced x-rays
Total beam energy	Calorimetry
Beam current	(i) Prompt γ-rays (ii) Biased ion collectors
Time-of-flight	(i) Prompt γ-rays (ii) Scintillator-photodiode (iii) Magnetic probes

Table 3 — Proton and Deuteron Induced Reactions

For producing β^+ activity

Reaction	Product half-life	Useful energy range (MeV)
$^{10}B(p,\gamma)^{11}C(\beta^+)^{11}B$	20.4 min.	$E_p \leq 1.145$ (resonance)
$^{12}C(p,\gamma)^{13}N(\beta^+)^{13}C$	9.96 min.	$E_p \leq 0.457$ (resonance)
$^{14}N(p,\gamma)^{15}O(\beta^+)^{15}N$	122 sec.	$E_p \geq 0.277$ (resonance)
$^{10}B(d,n)^{11}C(\beta^+)^{11}B$	20.4 min.	$E_d > 0.250$
$^{12}C(d,n)^{13}N(\beta^+)^{13}C$	9.96 min.	$E_d > 0.600$
$^{14}N(d,n)^{15}O(\beta^+)^{15}N$	122 sec.	$E_d > 0.700$

For producing neutrons

Reaction	Threshold (MeV)
$D(d,n)^3He$	---
$^9Be(p,n)^9B$	2.06
$^9Be(d,n)^{10}B$	---
$^9Be(\alpha,n)^{12}C$	---
$^{11}B(p,n)^{11}C$	3.0
$^{16}O(d,n)^{17}F$	1.83
$^{63}Cu(p,n)^{63}Zn$	4.21
$^{65}Cu(p,n)^{65}Zn$	2.17

For producing prompt γ rays

Reaction	Resonance Energy (KeV)
$^7Li(p,\gamma)^8Be$	441 1030 2060
$^{19}F(p,\alpha\gamma)^{16}O$	Many within range 227-1949

39

Table 4

Source

Average hollow beam radius at the anode (cm)	26
Magnetic Field (kG)	2.3
Pulse Duration (nsec)	70

Compression Region

	Before Compression	After Compression
Proton energy (MeV)	2	100
Magnetic field at M.P. (kG)	18.2	910
Proton current (MA)	0.92	46
Numer of protons	2×10^{17}	2×10^{17}
Ring kinetic energy (MJ)	0.064	3.?
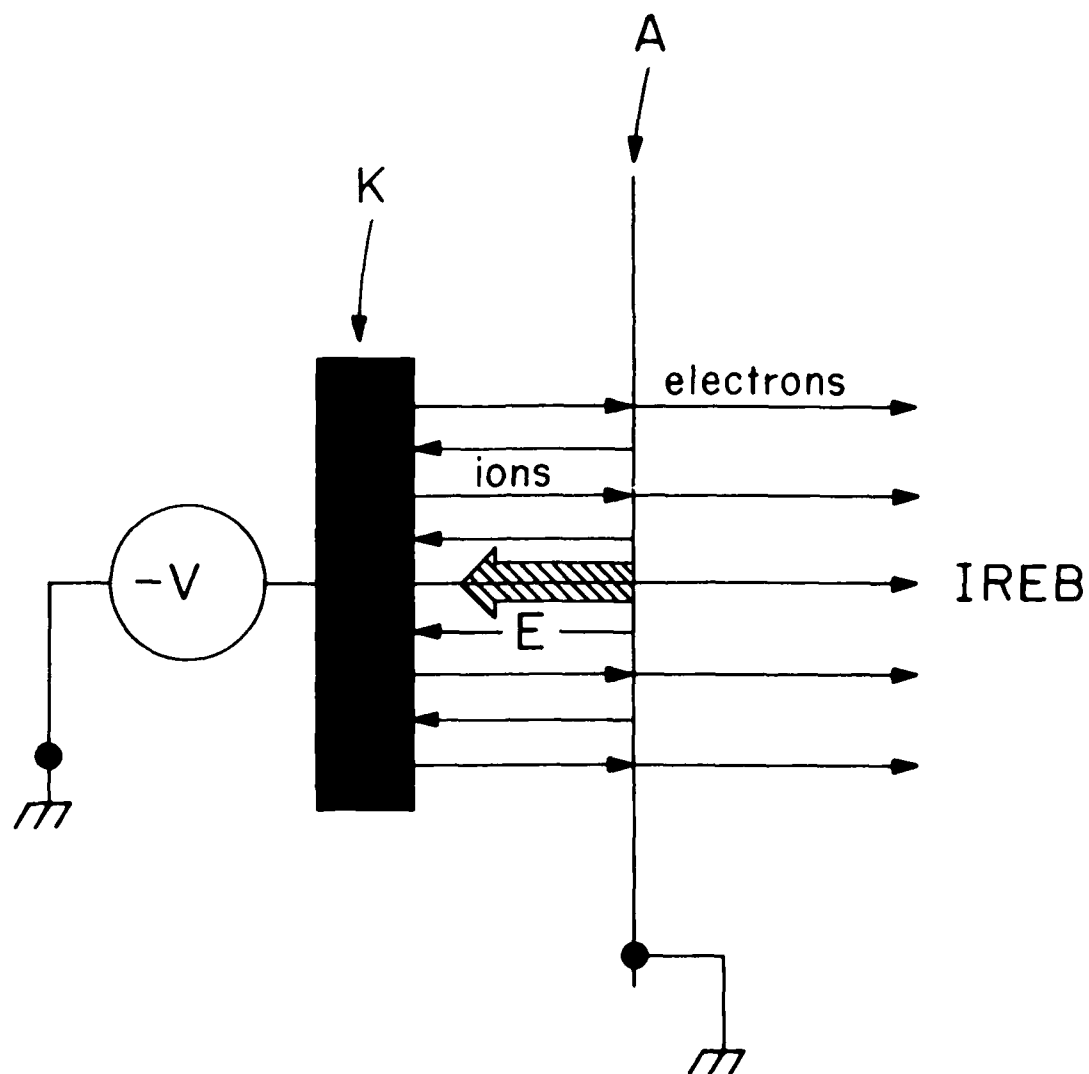
Figure 1 - The planar bipolar diode consisting of an anode (A) and a cath-
ode (K). Shown are the electrons, ions, and the electric field
(hatched arrow). Note that in principle, the ions could be ex-
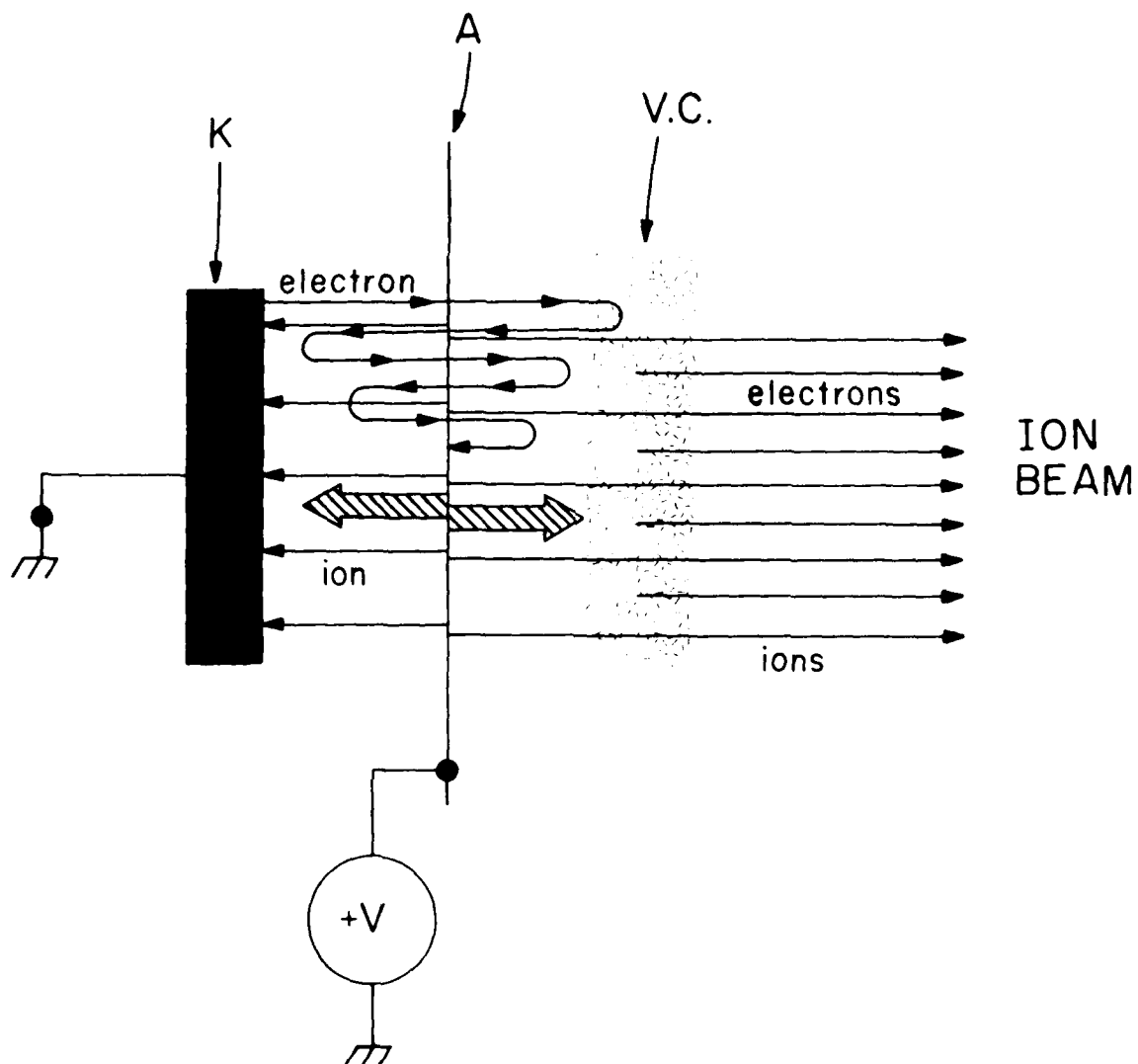tracted through a thin foil or screen cathode.

Figure 2 - Schematic of the reflex triode. The electrons emitted from
cathode (K) are shown reflexing about the anode (A) and forming
the virtual cathode (V.C.). The ions are accelerated by the
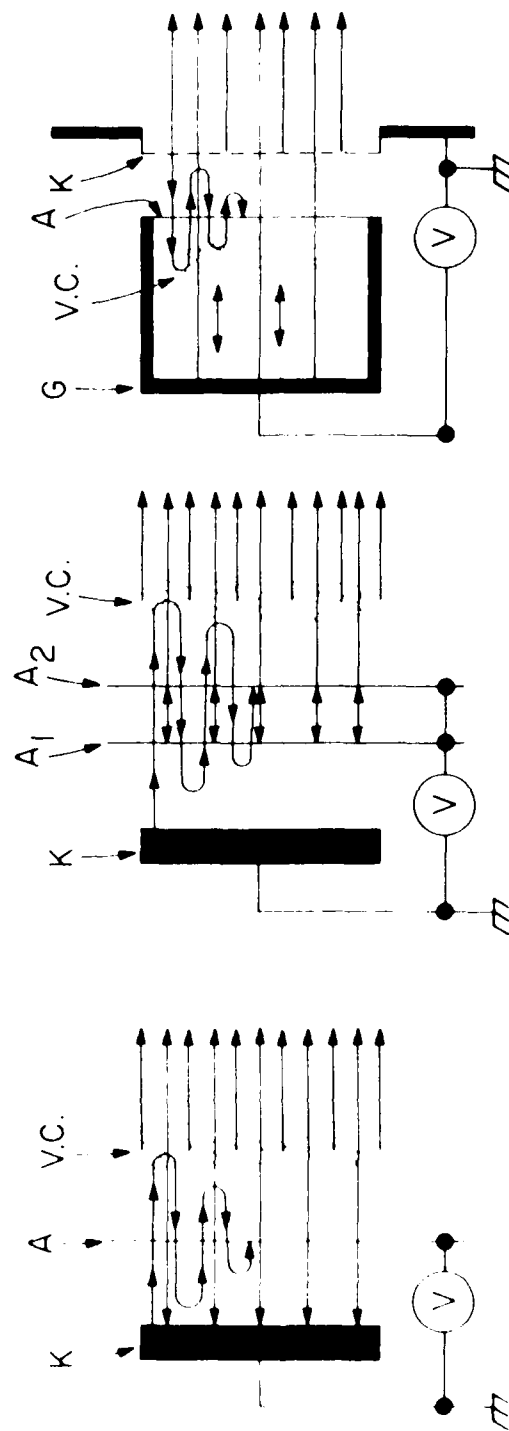electric field (hatched arrow) towards both the cathode and
virtual cathode.

Figure 3 - Schematic of the reflex triode (a), reflex tetrode (b), and inverse reflex tetrode (IRT) (c). Shown are the cathodes (K), the virtual cathodes (V.C.), the anodes (A, A_1, A_2), and electrons and the ions.
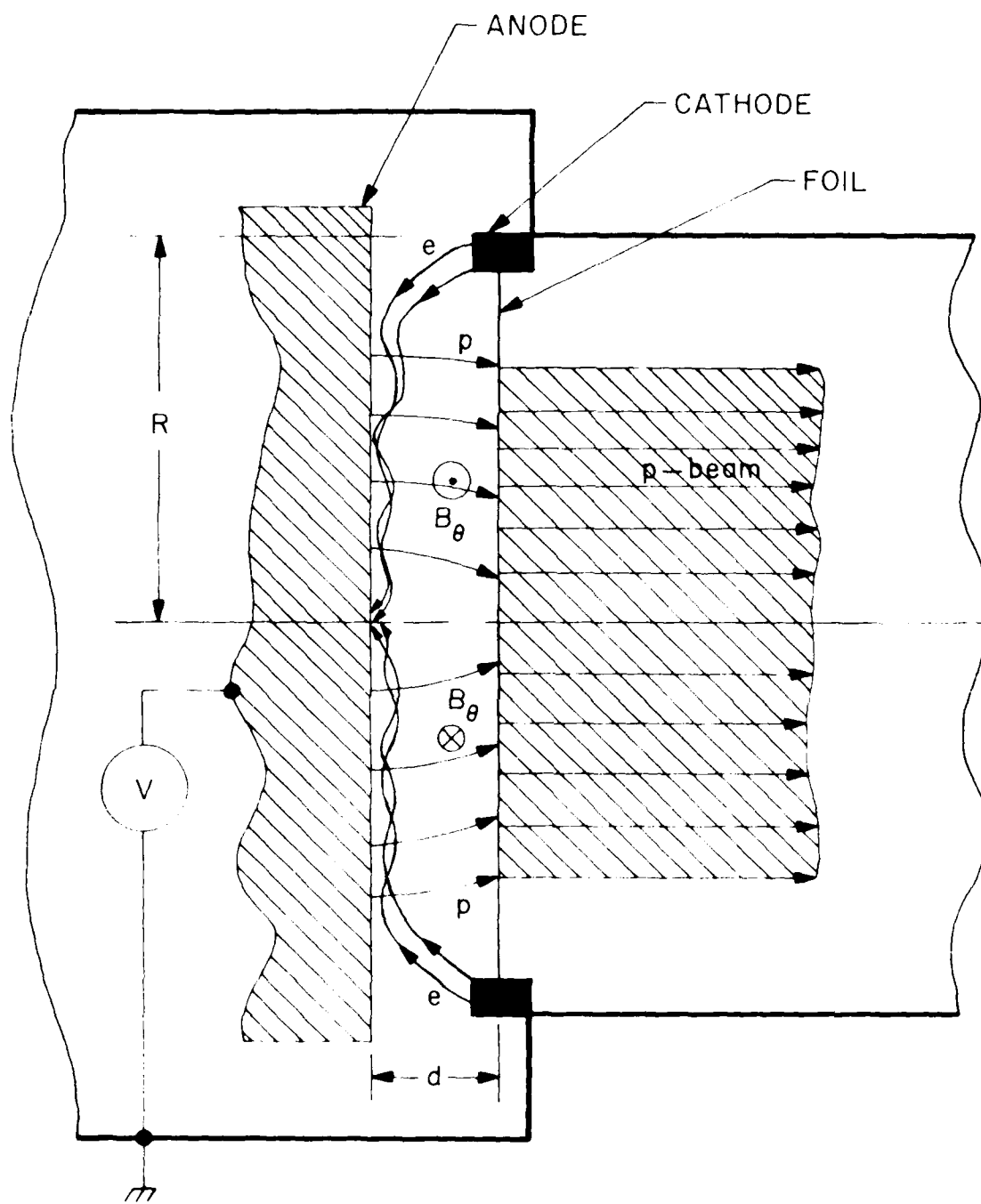
43

Figure 4 - Schematic of the pinched electron beam diode ion source.
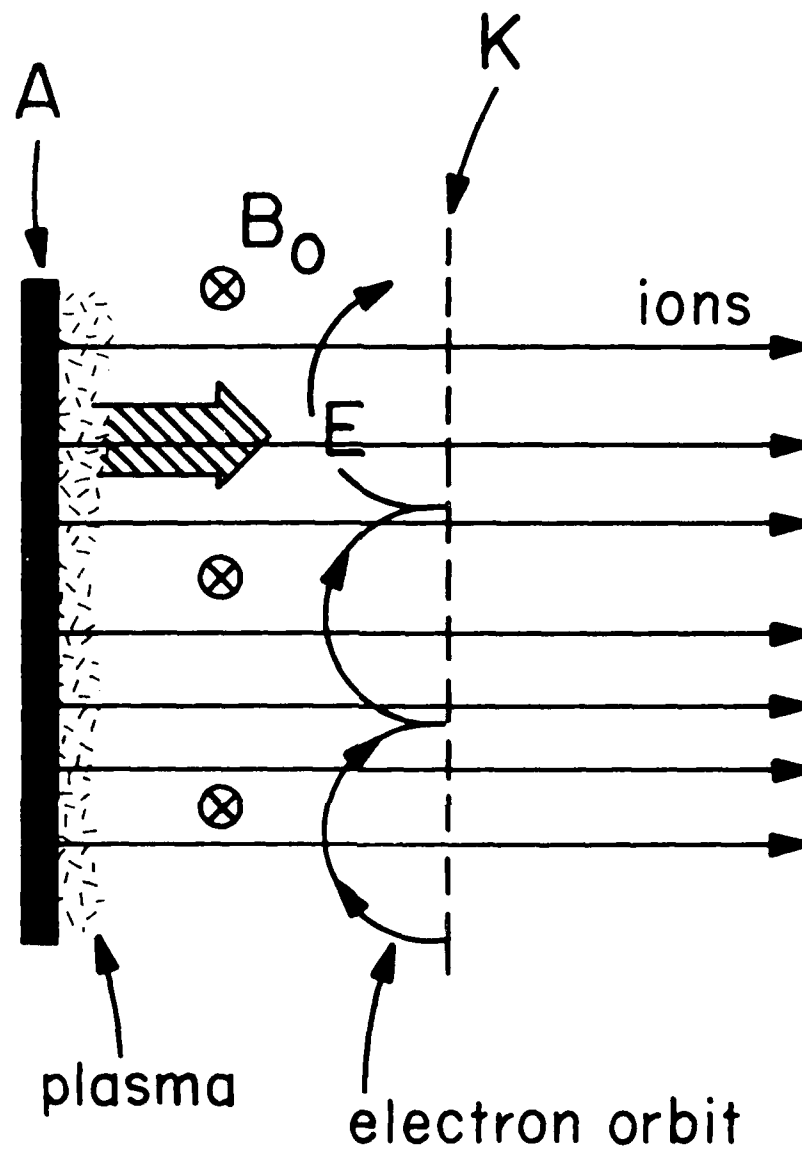
Figure 5 – The magnetically insulated diode consists of a cathode (K), an anode (A), and an applied magnetic field B_o which is strong enough to inhibit the electron flow from reaching the anode. Ions from the anode plasma are accelerated by the electric field (hatched arrow) and pass through the cathode forming a beam.
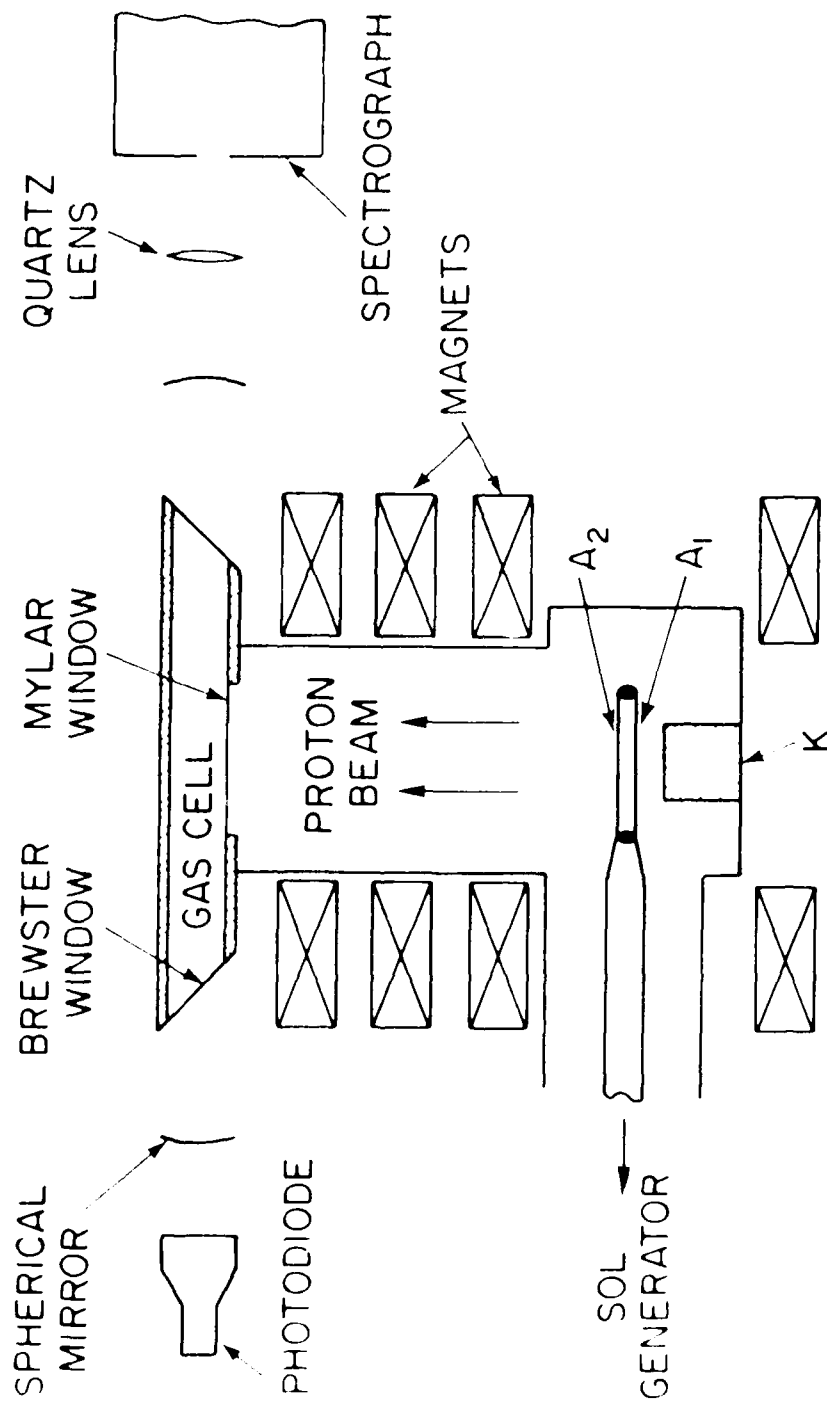
45

Figure 6 - Schematic diagram of the experimental apparatus used in the excitation of the first proton beam excited laser. Stimulated emission from an Ar/57, N_2 gas mixture was observed at $\lambda = 357.7$ and 380.5 mm.
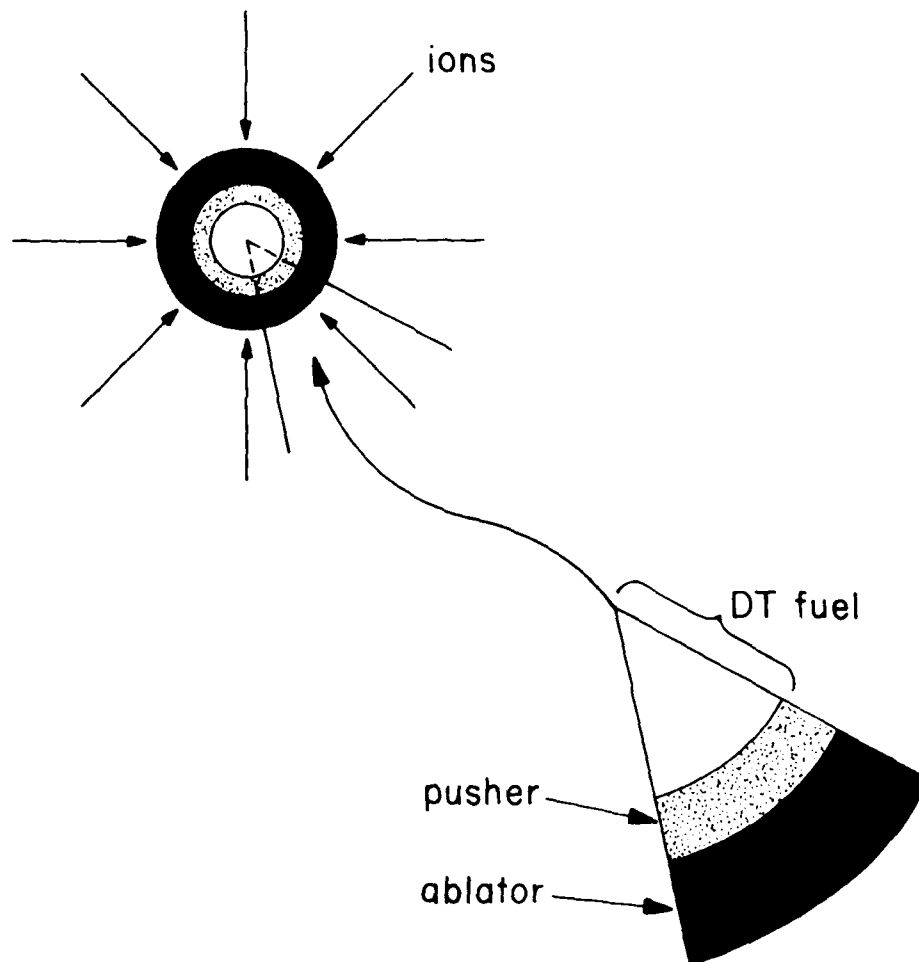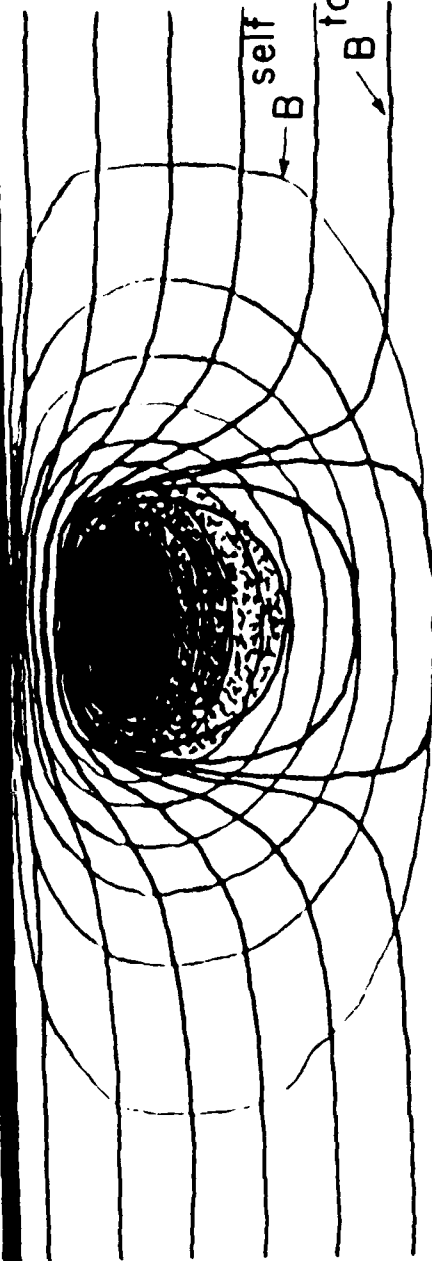
Figure 7 - Ion beam driven ICF. The ion beam ablates an outer layer of the
pellet. The exploding ablator (solid) transfers momentum to the
pusher (dotted) which compresses the DT fuel as it implodes.
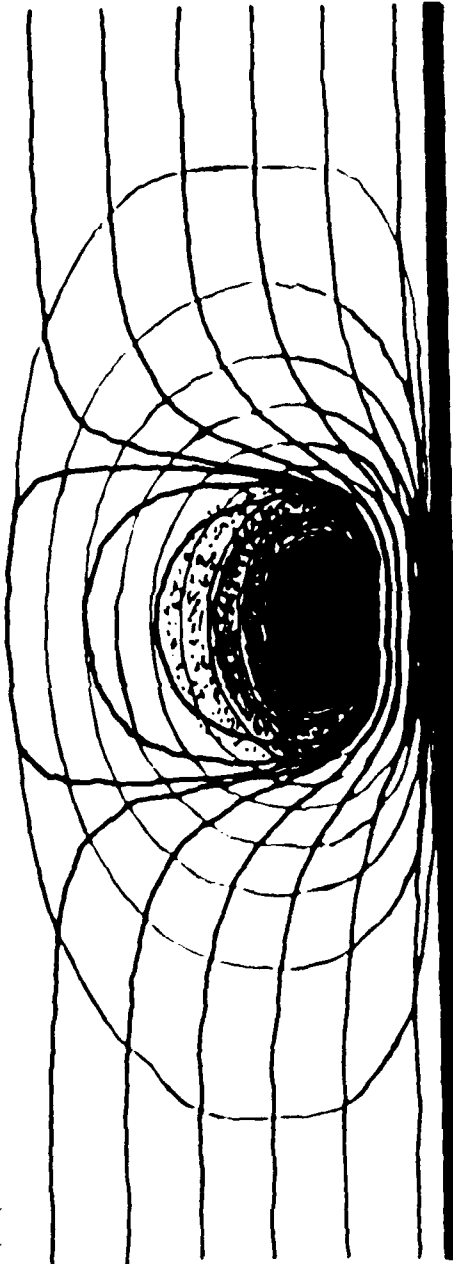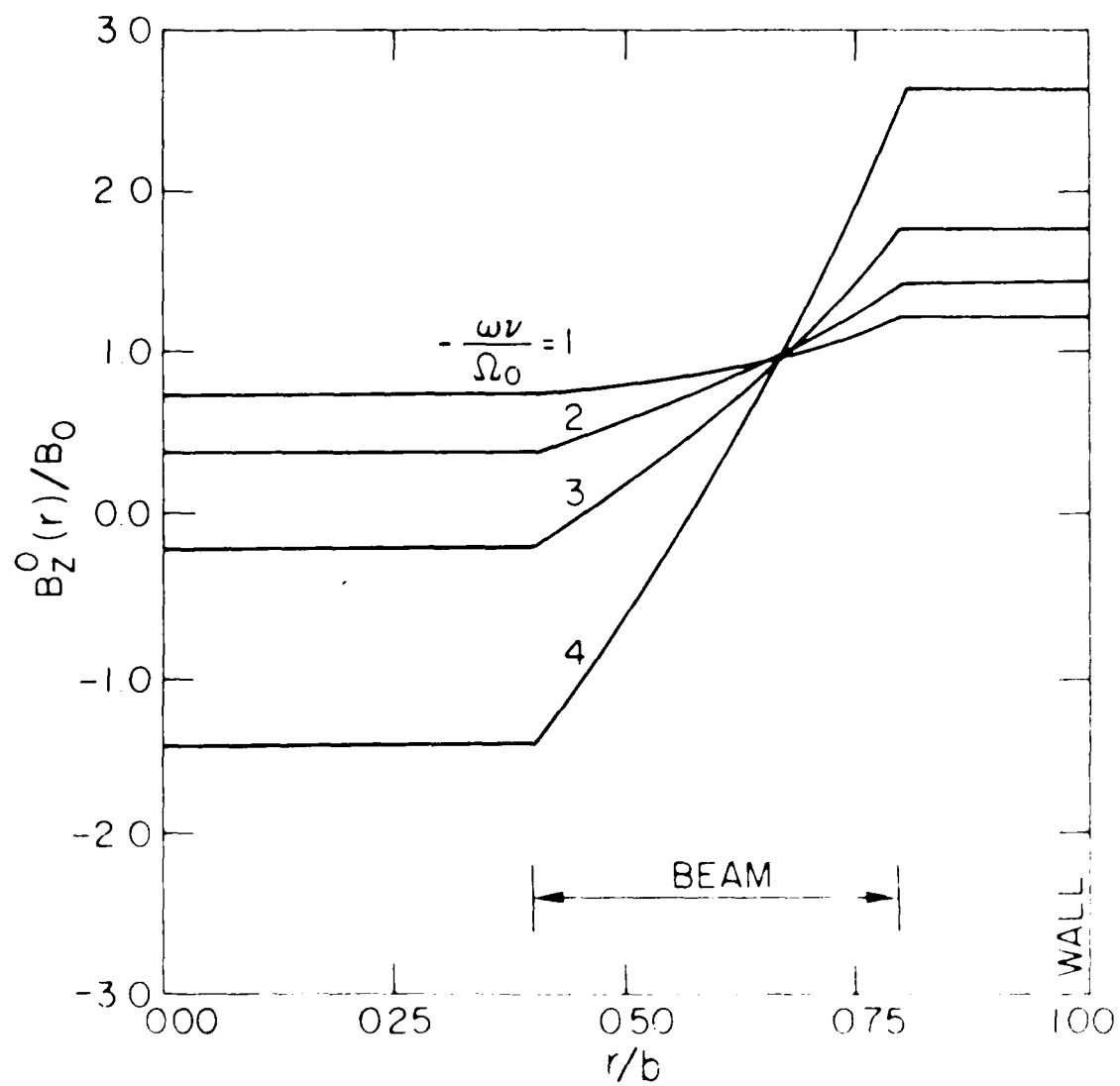
Figure 9 - Equilibrium magnetic field profiles for various values of the parameter $-\omega\nu/\Omega_0$. The ratios a/b and a/b are equal to 0.8 and 0.4 respectively.

49

GAMBLE
GENERATOR

MAGNETS

ON-AXIS B_z
MAGNETIC PROBE
CARBON
TARGET

G

K

A

B LOOPS

VOLTAGE
PROBE

CUSP

$B_\theta \& B_z$
MAGNETIC
PROBES

TEFLON TARGET

PROMPT γ-RAY
DETECTOR

.5 M
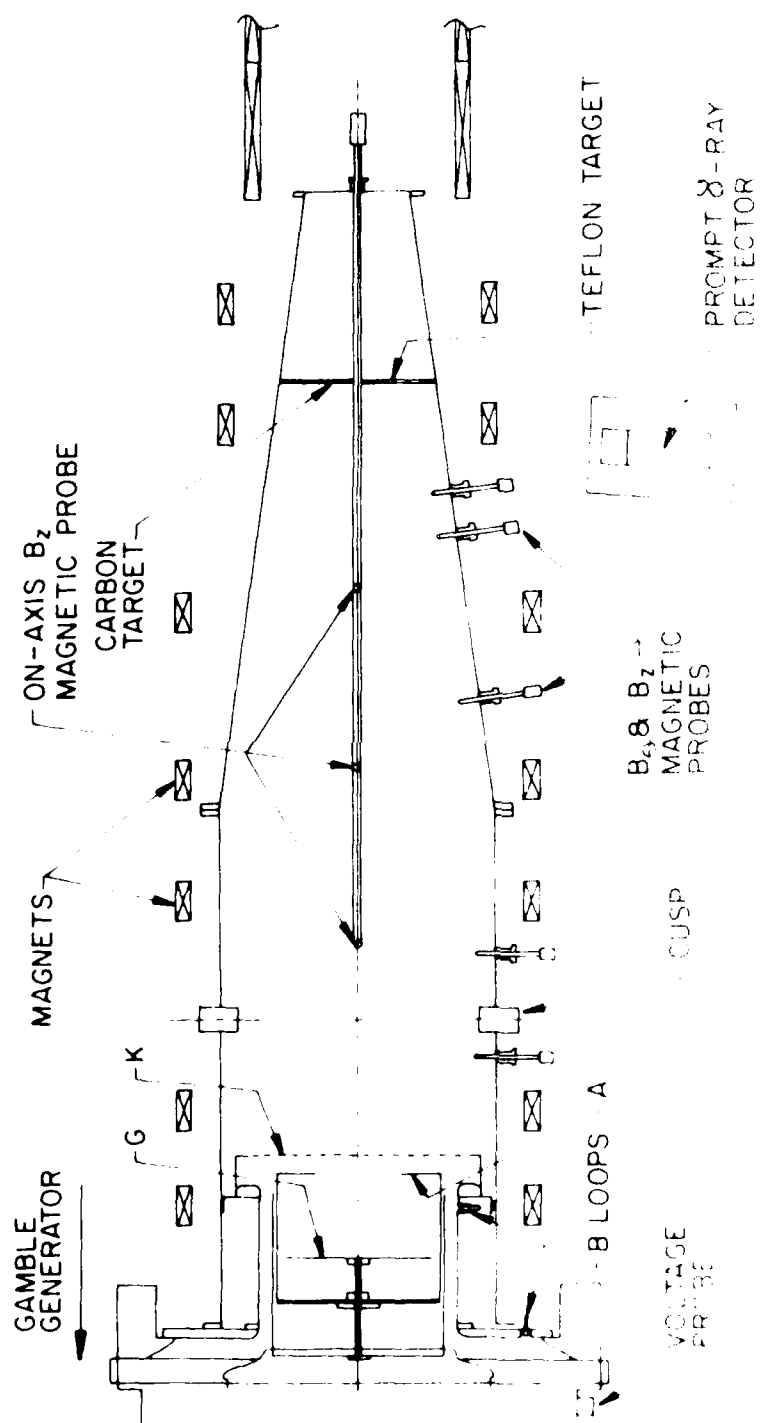
Fig. 21 - Photograph of a section of the NRL ion ring ex-
periment in front of the Gamble II generator.

Figure 12 - Illustration of the concept for generating a very high energy, high current ion beam. After it is compressed by a metal liner, the ring is extracted out through a half cusp, which partially unwinds the rotating ions.

DISTRIBUTION LIST

1. Prof. George Bekefi
   Bldg. 36-213
   Mass. Inst. of Technology
   77 Massachusetts Ave.
   Cambridge, Mass. 02139
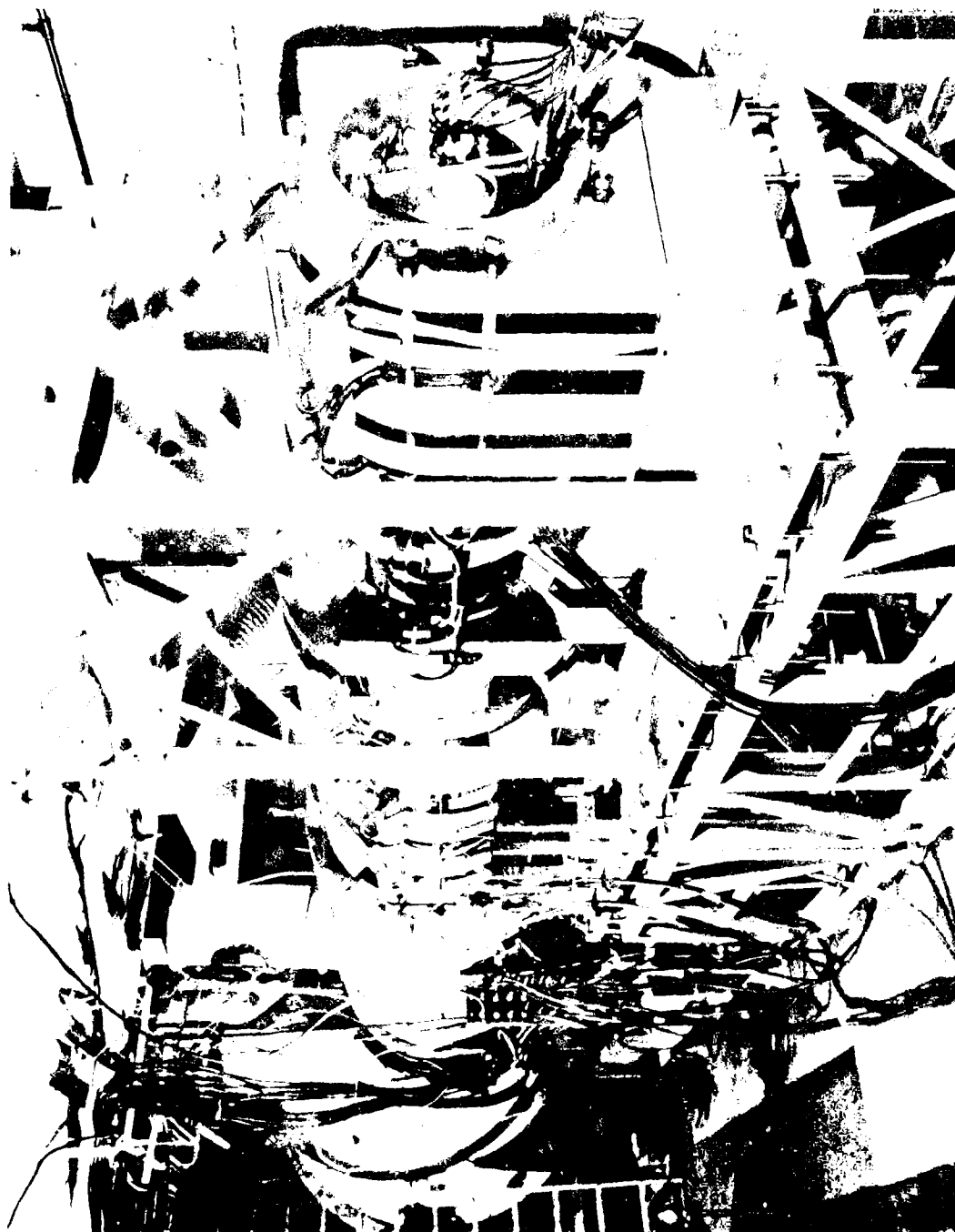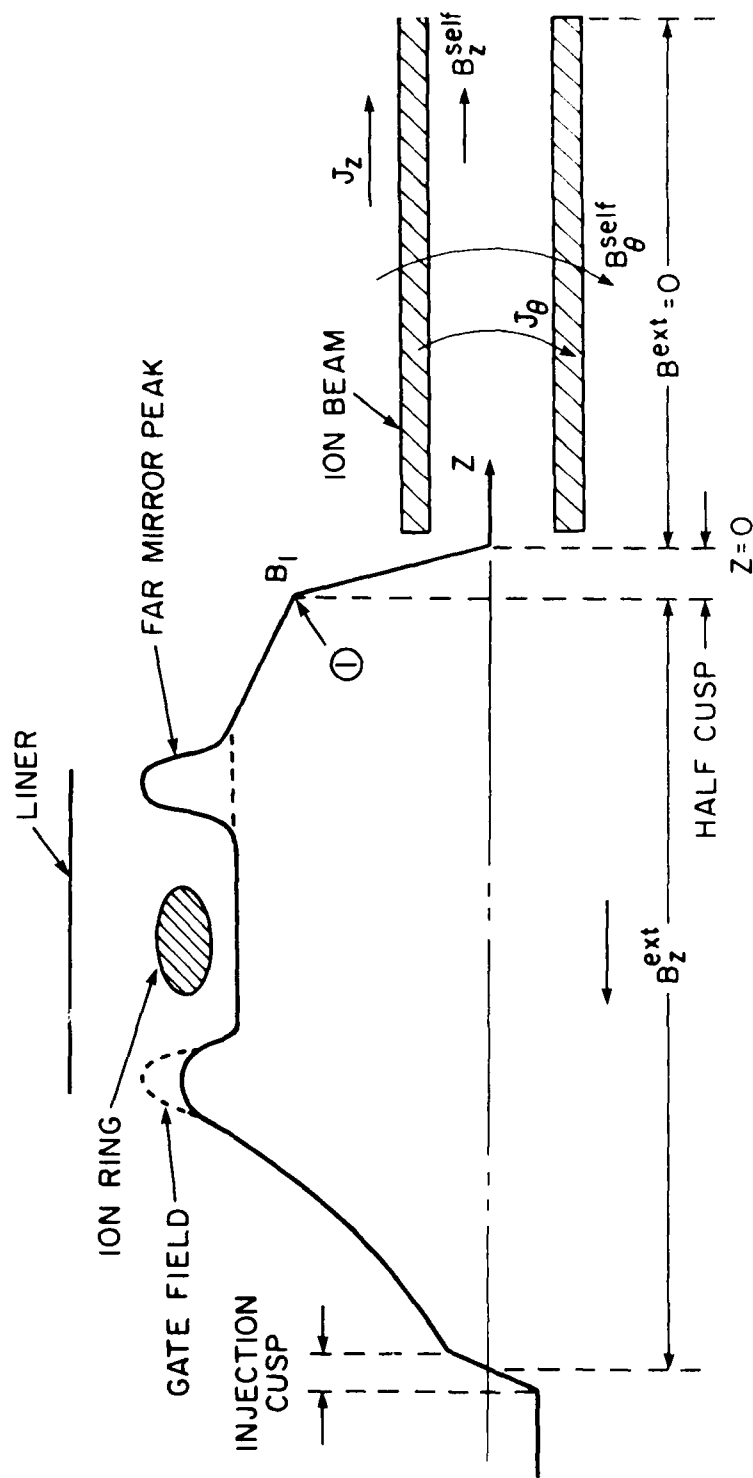
2. Dr. Jim Benford
   Physics International Co.
   2700 Merced St.
   San Leandro, CA 94577

3. Dr. Kenneth D. Bergeron
   Plasma Theory Div. - 5241
   Sandia Laboratories
   Albuquerque, Nex Mexico, 87115

4. Dr. V. M. Birtritsky
   Lenina 2a
   Research Institute of Nuclear Physics
   Tomsk, USSR

5. Dr. A. E. Blaugrund
   Weizman Institute of Science
   Rehovot, Israel

6. Dr. R. Briggs
   Lawrence Livermore Laboratory
   P. O. Box 808
   Livermore, CA 94550

7. Dr. Blake E. Cherrington
   Dept. of Electrical Engineering
   University of Illinois
   Urbana, IL 61801

8. Prof. G. Contopoulos
   Dept. of Astronomy
   University of Athens
   Athens, Greece

9. Prof. R. Davidson
   Plasma Fusion Center
   Massachusetts Inst. of Technology
   Cambridge, MA 02139

10. Dr. H. J. Doucet, Director
    Laboratoire de Physique
       des Milieux Ionises
    Ecole Polytechnique
    Plateau de Palaiseau
    91120 Palaiseau, France

11. Dr. W. Dove
    Dept. of Energy
    Washington, DC 20545

12. Dr. H. Dreicer
    Director
    Plasma Physics Division
    Los Alamos Scientific Lab.
    Los Alamos, N. M.   87544

13. Prof. W. E. Drummond
    Austin Research Associates
    1901 Rutland Drive
    Austin, TX 78758

14. Dr. A. Fisher
    Physics Dept.
    Univ. of California
    Irvine, Cal.   92664

15. Prof. H. H. Fleischmann
    Lab. for Plasma Studies and
       School of Applied and Engr. Physics
    Cornell University
    Ithaca, New York 14850

16. Dr. T. K. Fowler
    Assoc. Director for Magnetic
       Fusion Energy
    Lawrence Livermore Laboratory
    P. O. Box 808
    Livermore, CA 94550

17. Prof. D. Hammer
    Lab. of Plasma Studies
    Cornell University
    Ithaca, New York, 14850

18. Prof. R. Helleman
    Georgia Institute of Technology
    Atlanta, Georgia, 30332

19. Dr. S. Humphries
    Sandia Laboratories
    Albuquerque, New Mexico, 87115

20. Prof. H. Ishizuka
    Dept. of Physics
    Univ. of Tsukuba
    Ibaraki, 300-31, Japan

54

21. Prof. K. Karoumbalos
    Dept. of Physics
    University of Athens
    Athens, Greece

22. Dr. Takaya Kawabe
    Institute of Plasma Physics
    Nagoya University
    Nagoya 464
    Japan

23. Dr. J. D. Kilkenny
    Dept. of Physics
    Imperial College
    Prince Consort Road
    England

24. Dr. Peter Korn
    Maxwell Labs.
    San Diego, CA 92105

25. Dr. D. Lebedev
    Academy of Sciences of USSR
    P. N. Lebedev Physical Institute
    Moscow, Leninsky Prospect, 53 USSR

26. Prof. R. V. Lovelace
    School of Applied and Eng. Physics
    Cornell University
    Ithaca, New York, 14853

27. Dr. S. C. Luckhardt
    Plasma Fusion Center
    Mass. Inst. of Technology
    Cambridge, MA 02139

28. Prof. T. C. Marshall
    School of Eng. and Appl. Science
    Plasma Laboratory
    S. W. Mudd Bldg.
    Columbia Univ.
    New York, NY 10027

29. Dr. D. A. McArthur
    Sandia Lab.
    Albuquerque, New Mexico 87115

30. Prof. J. E. McCune
    Dept. of Aero. and Astro.
    Mass. Institute of Tech.
    77 Massachusetts Ave.
    Cambridge, Mass. 02139

31. Prof. G. H. Miley
     Chairman
     Nuclear Eng. Program
     214 Nuclear Eng. Lab.
     Urbana, IL 61801

32. Prof. A. Mohri
     Institute of Plasma Physics
     Nagoya University
     Nagoya, Japan

33. Dr. Ralph Moir
        L-386
     Lawrence Livermore Lab.
     P. O. Box 808
     Livermore, CA 94550

34. Prof. J. Nation
     Lab. of Plasma Studies
     Cornell University
     Ithaca, NY 14850

35. Dr. Joan Ogden
     Princeton Plasma Lab.
     Princeton, New Jersey

36. Dr. C. L. Olson
     Sandia Lab.
     Albuquerque, New Mexico 87115

37. Dr. I. I. Pervushin
     Academy of Sciences of USSR
     Radiotechnical Institute
     " Marta Str. 1 -12
     12,086 Moscow A-85, USSR

38. Dr. R. Post
     Lawrence Livermore Laboratory
     University of California
     P. O. Box 808
     Livermore, CA 94550

39. Dr. D. S. Prono
     Lawrence Livermore Laboratory
     P. O. Box 808
     Livermore, CA 94550

40. Dr. S. Putnam
     Physics Intern. Co.
     2700 Merced St.
     San Leandro, CA 94577

56

41. Prof. N. Reiser
    Dept. of Physics and Astronomy
    University of Maryland
    College Park, MD 20742

42. Dr. M. E. Rensink
    Lawrence Livermore Laboratory
    University of California
    P. O. Box 808
    Livermore, CA 94550

43. Mr. D. Rej
    Lab for Plasma Studies
    Cornell University
    Ithaca, NY 14853

44. Dr. J. A. Rome
    Oak Ridge National Lab.
    Oak Ridge, Tenn. 37850

45. Prof. Norman Rostoker
    Dept. of Physics
    University of California
    Irvine, CA 92664

46. Dr. L. I. Rudakov
    I. V. Kurchatov Institute of Atomic Energy
    Moscow, USSR

47. Prof. D. D. Ryutov
    Sibirian Branch of Academy of Science
        of U. S. S. R.
    Institute of Nuclear Physics
    Navosibirsk, USSR

48. Prof. Hans Schamel
    464 Bochum -
    RUHR-Universität W. Germany

49. Prof. George Schmidt
    Physics Dept.
    Stevens Institute of Technology
    Hoboken, New Jersey 07030

50. Prof. P. Seraphim
    Electrical Eng. Dept.
    National Technical Univ. of Athens
    Athens, Greece

51. Prof. R. Sudan
    Lab. of Plasma Studies
    Cornell University
    Ithaca, New York 14850

52. Prof. A. W. Trivelpiece
     Science Applications, Inc.
     San Diego, CA 92123

53. Dr. S. S. Tserevitinov
     Kurchatov's Institute of Atomic Energy
     Moscow, USSR

54. Prof. R. Uzan
     Laboratoire D'emission Electronique
     Faculte des Sciences
     43, Bd du 11 Novembre 1918
     69 - Villeurbanne, France

55. E. S. Weibel
     c/o Center de Recherches
       en Physique des Plasmas
     Ecole Polytechnique Federale
       de Lausanne
     Avenue des Bains 21
     CH-1007, Lausanne, Switzerland

56. Prof. C. B. Wharton
     Occidental Research Corp.
     2100 SE Main Street
     Irvine, CA 92713

57. Dr. Gerold Yonas
     Sandia Lab.
     Albuquerque, NM 87115

58. Prof. A. Bers
     Dept. of Electrical Engr.
     Mass. Inst. of Technology
     77 Massachusetts Ave.
     Cambridge, Mass. 02159

59. Dr. Charles C. Damm
     Lawrence Livermore Laboratory
     P. O. Box 808
     Livermore, CA 94550

60. Dr. Chip Smith Jr.
     Pacific Gas and Electric Co.
     77 Beale Street
     San Francisco, CA 94106

61. Dr. G. P. Gupta
     Scientific Officer
     Bhabha Atomic Research Centre
     (MHD Generation Project)
     Bombay, India 400085

62. Dr. A. N. Didenko
Inst. of Nuclear Physics
Tomsk, USSR

63. Dr. A. C. Kolb
Maxwell Lab., Inc.
San Diego, CA 92123

64. Dr. J. Lawson
Univ. of California at
Los Angeles
Dept. of Physics
Los Angeles, CA 90024

65. Dr. R. Linford
Los Alamos Scientific Lab.
P.O. Box 1663
Los Alamos, NM 87545

66. Dr. C.S. Liu
Dept. of Physics
University of Maryland
College Park, MD 20742

67. Dr. J. McNally, Jr.
Oak Ridge National Lab.
P.O. Box Y
Oak Ridge, TN 37830

68. Dr. W. H. Ellis
Chief Magnetic Mirror Systems
Office of Fusion Energy
Dept. of Energy
Washington, D.C. 20545

69. Dr. A. Bromborsky
Harry Diamond Lab.
2800 Powder Mill Rd.
Adelphi, MD 20783

70. Dr. V.P. Sarantsev
Jt. Institute for Nuclear Res.
Head Post Office P.B. 79, Moscow
Dubna, USSR

71. Dr. B. Godfrey
Mission Res. Corp.
1400 San Mateo Blvd. S.E.
Suite A
Albuquerque, NM 87108

72. Prof. C. Striffler
    Dept. of E.E.
    Univ. of Maryland
    College Park, MD 20742

73. Dr. R.J. Faehl
    Los Alamos Scientific Lab.
    Los Alamos, NM 87544

74. Dr. W. Condit
    Div. Appl. Plasma Physics
    U.S. Dept. of Energy
    Washington, D.C. 20545

75. Dr. J.M. Buzzi
    Ecole Polytechnique
    Plateau de Palaiseau
    91120 Palaiseau, France

76. Dr. A. Miyahara
    Institute of Plasma Physics
    Nagoya Univ.
    Nagoya 464
    Japan

77. Dr. Shigeo Kawata
    Tokyo Inst. of Technology
    Tokyo, Japan

78. Dr. D.A. Johnson
    Sandia Nat'l Lab.
    Albuquerque, NM 87115

79. Prof. F. Chen
    Dept. of E.E.
    Univ. of Calif. at Los Angeles
    Los Angeles, Calif. 90024

80. Mr. J.E. Maenchen
    Physics International Co.
    2700 Merced St.
    San Leandro, CA 94577

81. Dr. Z.G.T. Guiragossian
    TRW Sys. and Energy R1/1070
    Advanced Technology Lab.
    1 Space Park
    Redondo Beach, CA 90278

82. Dr. S. Graybill
    Harry Diamond Lab.
    2800 Powder Mill Rd.
    Adelphi, MD 20783

83. Dr. J. Sazama
    Naval Surface Weapons Center
    Code 431
    White Oak, Silver Spring, MD 20910

84. Dr. J.U. Guillory
    Jaycor
    20550 Whiting St.
    Suite 500
    Alexandria, VA 22304

85. Dr. A. Sternlieb
    Lawrence Berkely Lab.
    Berkeley, CA 94720

86. Dr. M. Masumaki
    Inst. of Plasma Physics
    Nagoya University
    Nagoya, Japan

87. Dr. D. Straw
    AFWL
    Kirtland AFB, NM 87117

88. Dr. H. Uhm
    Naval Surface Weapons Center
    White Oak, Silver Spring, MD 20910

89. Dr. J.G. Eden
    Dept. of Electrical Engineering
    Univ. of Illinois
    155 EEB
    Urbana, Ill. 61801

90. Prof. W. Doggett
    NC State Univ.
    P.O. Box 5342
    Raleigh, NC 27650

91. Prof. B. Dangor
    Dept. of Physics
    Imperial College of Science and Technology
    London S.W.7 England

92. Dr. Venkat Ramani
    554 Exp'l Plasma Physics
    Phys. Res. Lab.
    Navrangpura Ahmedabad -380-009
    India

93. Dr. C.A. Patou
    Ctr. D'Etudes Valduc
    B.P. 14
    21120 Is Sur Tillie, France

94. Dr. A. Kolomensky
    Lebedeu Physical Institute
    Moskow, USSR

95. Dr. Jen-Chang Chou
    Institute of Nuclear Energy Research
    P.O. Box 3
    Lung-Tan, Taiwan

96. Dr. M. Caponi
    TRW Advance Tech. Lab.
    1 Space Park
    Redondo Beach, CA   90278

97. Dr. F.J. Castleberry
    Defense Intelligence Agency
    Attn. DT-IA
    Washington, D.C.   20301

98. Dr. W.N. Destler
    Dept. of Electrical Engineering
    Univ. of Maryland
    College Park, MD   20742

99. Dr. C.E. Hollandsworth
    Ballistic Research Lab.
    DRDAB - BLB
    Aberdean Proving Ground, MD   21005

100. Dr. M. Nahemow
     Westinghouse Electric Corp.
     1310 Beutah Rd.
     Pittsburgh, PA   15235

101. Dr. W.S. Applegate
     CIA
     Washington, D.C.   20505

102. Dr. J. Boyle
     DARPA/tni. 28
     1400 Wilson Blvd.
     Arlington, VA 2...

103. Dr. J. Hyman
     Hughes Research Lab.
     3011 Malibu Cyn Rd.
     Malibu, CA 90265

104. Defense Technical Information Center (DTIC)
     Cameron Station
     5010 Duke Street
     Alexandria, VA 22314

105. Naval Research Laboratory
     Washington, D.C. 20375

          Code 2628 - 20 cpys

          Code 4700 - 25 cpys

          Code 4761 - 75 cpys

DATE
ILMED
8